



Adverse Weather Scenarios for Future Electricity Systems:

Characterising short-duration ramping events (including addendum)

Author(s): Megan Pearce, Dr Laura Dawkins and Isabel Rushby

Reviewed by: Dr Emily Wallace

Prepared for: National Infrastructure Commission

Revision Date: February 2022

If printing double-sided you will need this blank page. If printing single sided, please delete this page

Revision History

VERSION	DESCRIPTION	AUTHOR	REVIEWER	APPROVED
FINAL (OCT 2021)	Revisions finalised and published	Megan Pearce,	Emily Wallace	Emily Wallace
FINAL_WITHADDENDUM (DEC 2021)	Additional sensitivity studies added	Laura Dawkins Megan Pearce, Laura Dawkins, Isabel Rushby	Emily Wallace	Emily Wallace
FINAL_WITHADDENDUM_REVISIED (FEB 2022)	Revisions made to remove spurious midnight ramps	Megan Pearce, Laura Dawkins, Isabel Rushby	Emily Wallace	Emily Wallace

Disclaimer

- This document is published by the Met Office on behalf of the Secretary of State for Business, Energy and Industrial Strategy, HM Government, UK. Its content is covered by © Crown Copyright 2022.
- This document is published specifically for the readership and use of National Infrastructure Commission and may not be used or relied upon by any third party, without the Met Office's express written permission.
- The Met Office aims to ensure that the content of this document is accurate and consistent with its best current scientific understanding. However, the science which underlies meteorological forecasts and climate projections is constantly evolving. Therefore, any element of the content of this document which involves a forecast or a prediction should be regarded as our best possible guidance, but should not be relied upon as if it were a statement of fact. To the fullest extent permitted by applicable law, the Met Office excludes all warranties or representations (express or implied) in respect of the content of this document.
- Use of the content of this document is entirely at the reader's own risk. The Met Office makes no warranty, representation or guarantee that the content of this document is error free or fit for your intended use.
- Before taking action based on the content of this document, the reader should evaluate it thoroughly in the context of his/her specific requirements and intended applications.
- To the fullest extent permitted by applicable law, the Met Office, its employees, contractors or subcontractors, hereby disclaim any and all liability for loss, injury or damage (direct, indirect, consequential, incidental or special) arising out of or in connection with the use of the content of this document including without limitation any and all liability:
 - relating to the accuracy, completeness, reliability, availability, suitability, quality, ownership, non-infringement, operation, merchantability and fitness for purpose of the content of this document;
 - relating to its work procuring, compiling, interpreting, editing, reporting and publishing the content of this document; and
 - resulting from reliance upon, operation of, use of or actions or decisions made on the basis of, any facts, opinions, ideas, instructions, methods, or procedures set out in this document.
- This does not affect the Met Office's liability for death or personal injury arising from the Met Office's negligence, nor the Met Office's liability for fraud or fraudulent misrepresentation, nor any other liability which cannot be excluded or limited under applicable law.
- If any of these provisions or part provisions are, for any reason, held to be unenforceable, illegal or invalid, that unenforceability, illegality or invalidity will not affect any other provisions or part provisions which will continue in full force and effect.

Contents

Revision History	3
Disclaimer	4
Contents	5
Executive Summary	6
1 Introduction	8
2 Summary of Phase 2	10
Phase 2(a): Characterising long-duration adverse weather events	10
Phase 2(b): Developing the dataset of long-duration events	11
3 Characterising short-duration ramping events	12
2.1 Estimating wind electricity capacity factor	12
2.2 Estimating solar electricity capacity factor	15
3.1 Calculating the change in capacity factor over time windows	17
3.2 Extreme Value Analysis	18
3.3	
3.4 Results	20
4.1 Wind	20
4.1.1 Maximum change in capacity factor in Great Britain over various time windows 20	
4.1.2 Maximum change in capacity factor across defined regions over various time windows 22	
4.2 4.1.3 Return periods and return levels of extreme events	28
Solar	33
4.2.1 Maximum change in capacity factor across defined regions over various time windows 33	
4.2.2 Return periods and return levels of extreme events	39
5 Summary and Conclusion	43
6 References	46
9.17 Glossary	48
9.2 8 Appendix	49
9 Addendum	68
Region sensitivity study	68
Euro4 wind ramping validation	73

Executive Summary

The first National Infrastructure Assessment (National Infrastructure Commission, 2018), published by the National Infrastructure Commission (the Commission) in 2018, recommends targeting a transition of the UK electricity system to a highly renewable generation mix, incorporating increasing wind and solar power capacities. This is consistent with a number of other recent reports such as the Climate Change Committee's Sixth Carbon Budget report (Climate Change Committee, 2020), and the International Energy Agency's Net Zero by 2050 Roadmap for the Global Energy Sector (International Energy Agency, 2021), all reflecting the need for a de-carbonised energy system to help tackle the climate crisis.

Whilst desirable, transitioning to this highly renewable mix will increase the vulnerability of the UK's electricity system to adverse weather conditions, such as sustained periods of low wind speeds leading to low wind generation, coupled with cold winter or high summer temperatures leading to peak electricity demand, or short-duration changes in wind speed or solar radiation that can result in rapid, instantaneous changes in generation. Consequently, the Commission want to improve understanding of the impact of adverse weather conditions on a highly-renewable future system. This will support the recommendations it makes to government and provide beneficial inputs to those that model and design future electricity systems.

To improve this understanding, the Met Office have been working with the National Infrastructure Commission and Climate Change Committee to develop two datasets of adverse weather scenarios, based on physically plausible weather conditions, representing a range of possible extreme events, and the effect of future climate change. These datasets will allow for proposed future highly renewable electricity systems to be stress tested to evaluate resilience to challenging weather and climate conditions. The first of these datasets, published to the Centre for Environmental Data Analysis (CEDA) archive¹ in June, focuses on long-duration adverse weather scenarios and characterises winter-time and summer-time wind-drought-peak-demand events, and summertime surplus generation events, in the UK and in Europe.

This report presents the first phase of development and validation of methods for characterising short-duration adverse weather stress events in the UK. Short-duration adverse weather scenarios are characterised by a large change in energy generation in a small time-window, known as ramping events. This characterisation will allow for wind and solar ramping events to be identified within any suitable meteorological data record, as required in future

¹ <https://catalogue.ceda.ac.uk/uuid/7beeed0bc7fa41feb10be22ee9d10f00>

phases of this project. The method is applied to 36 years of historical meteorological data and the resulting adverse weather events within the historical report are presented.

Using insights from the electricity modelling literature, the developed method estimates wind and solar capacity factors across Great Britain, using wind speed data at turbine hub height as well as incoming solar radiation and temperature, respectively. The capacity factors are then aggregated by splitting Great Britain into smaller regions for onshore wind, offshore wind and solar to reflect the climatological variation of meteorological variables. A short-duration ramping event for a given region, was then quantified as the maximum change in capacity factor, within a given time window – an approach adopted from Cannon et al. (2015). The time windows explored are those used by Cannon et al. (2015): 1 hour, 3 hours, 6 hours, 12 hours and 24 hours. For a given time window (e.g., 3 hours) and region (e.g., Scotland), the number of times this ‘maximum capacity factor change’ surpasses a particular change threshold was calculated. The average number of ramping events per year that surpass each change threshold of interest for a given time window was determined for Great Britain, to allow a comparison with the results of Cannon et al. (2015), as well as the defined wind and solar regions. Characterising events with this approach provides insight into the frequency of different size ramping events in any suitable meteorological dataset.

The results presented for wind ramping events are consistent with those produced by Cannon et al. (2015), although some small variation exists due to differing turbine allocation assumptions. Additionally, this work has expanded the scope of the Cannon et al. (2015) by using the approach to characterise solar ramping events. However, improvements for future work (not within the scope of this project) have been identified in order to better capture the weather driven ramping (i.e. changes to solar generation not just due to the sun rising and setting). It was found that these solar weather driven ramping events were not captured due to their occurring on a smaller scale than the regions used for this analysis.

Finally, an extreme value analysis was used to identify the 1 in 2, 5, 10, 20 and 30-year return period wind and solar ramping events for each region and time window combination. Examples of short-duration wind and solar ramping events identified in the historical period are then presented.

1 Introduction

The Met Office are developing a dataset of adverse weather events that can be used by energy system modellers to test the weather and climate resilience of potential future highly renewable electricity systems. To date, the project has involved; an initial literature review (Dawkins, 2019), a project scoping report (Butcher and Dawkins, 2020), the characterisation of long-duration adverse weather stress events (Dawkins and Rushby, 2021) and the development of the ‘Adverse Weather Scenarios for Future Electricity Systems’ dataset of long-duration events (Dawkins et al., 2021a) and associated report (Dawkins et al., 2021b).

This report presents the methods developed to characterise short-duration adverse weather stress events in the UK. Short-duration adverse weather scenarios are characterised by a large change in energy generation in a small time-window, known as ramping events. A wind ramping event is characterised by large changes in wind speed, and subsequent wind power production, during a short time window. The frequency and severity of such events, which are often associated with low pressure weather systems passing over the UK, have been explored by Cannon et al. (2015). They also note that ramping often occurs at moderate wind speeds but, in more rare cases, can also occur during extremely high wind speeds when turbines shut down for safety (Sinden, 2007). These events are most frequent and extreme in autumn and winter due to the occurrence of windstorms over Europe during these months (Cannon et al., 2015) and are found to be most common in September and October, when wind speed (and hence wind power generation) approaches its winter maximum level, while demand remains moderate (Bloomfield et al., 2018). Historical case study events indicate the potential for wind capacity factor to change by 80% in a 3-hour time window and hence a future energy system that has an increased installed wind capacity will be more vulnerable to the variability in power supply from wind ramping events (Drew et al., 2017).

Wind is a highly variable element whose magnitude can change dramatically depending on local climatology and terrain (Watson, 2014). Burton et al. (2011) explains how these local variations in topology and climatology lead to turbulence, defined as fluctuations in wind speed on a relatively fast time scale. Therefore, capturing local variations in wind speeds is important when characterising ramping stress events. Similarly, solar ramping events, characterised by large instantaneous fluctuations in solar irradiance (solar radiation reaching the surface) impacting on solar power production, are the result of local variability. Lohmann et al. (2016) found that mixed sky conditions are shown to have higher probabilities of strong fluctuations in solar irradiance, compared with overcast and clear skies, and are therefore most potentially problematic in terms of local short-term variability in irradiance increments (changes over specified intervals of time). Historical case study events demonstrate how multiple

instantaneous fluctuations in solar irradiance can be experienced within a few minutes (Lohman et al., 2016). To better capture the smaller scale meteorological conditions relevant for such energy ramping events, this phase of the project utilises the Euro4 hindcast dataset, which provides a much higher spatial resolution (4 km) representation of the historical period 1979-2014, compared to the ERA5² reanalysis dataset (30 km) used in Phase 2. Whilst Euro4 offers a significant improvement upon previous reanalysis products to move towards smaller scale features, it will not resolve finer scale conditions which can be of interest, such as individual clouds and turbulence. This is a limitation of the modelling. The hourly Euro4 hindcast data was generated by the Met Office using the European Atmospheric Hi-Res³ forecasting model, driven by ERA-Interim reanalysis data, to create a downscaled hindcast (i.e. a historical forecast) dataset at 4km resolution.

Cannon et al. (2015) explore the frequency of rapid change wind ramping events in the UK (1980-2012) by calculating the frequency of hours for which there is a subsequent ramp in generation of at least ΔCF (change in capacity factor) within a given time window. This phase of the project will use the Cannon et al. (2015) method (for calculating changes in capacity factor over various time windows) in combination with methods developed in the previous phase (for estimating wind and solar energy capacity factors from meteorological data) to characterise short-duration wind and solar ramping events in Great Britain. Firstly, this report will briefly summarise the approach developed for characterising long-duration adverse weather scenarios, as previously published in Dawkins and Rushby (2021). The application of the relevant method sections, and those explored in Cannon et al. (2015), to characterise wind and solar ramping events are then described. The exploration of historical wind and solar ramping events is presented, and then finally, tables of short-duration wind and solar ramping events identified in the historical period are provided.

In a later stage of this phase and in line with the previous Phase 2 approach, these methods will be applied to the UK Climate Projections (UKCP18) (Lowe et al., 2018). This will be used to consider how ramping-relevant weather conditions are likely to change in the future as a result of climate change. Finally a dataset of short duration events will be produced, capturing various extreme and climate warming levels. The details of this will be provided in a separate report.

² <https://www.ecmwf.int/en/forecasts/datasets/reanalysis-datasets/era5> (Accessed: 17th August 2021)

³

https://www.metoffice.gov.uk/binaries/content/assets/metofficegovuk/pdf/data/european_model_data_sheet_lores1.pdf (Accessed: 17th August 2021)

2 Summary of Phase 2

Phase 2(a): Characterising long-duration adverse weather events

The Phase 2 (a) report (Dawkins and Rushby, 2021) presents the development and validation of an approach for characterising adverse weather events using meteorological data, focusing on long-duration wind-drought-peak-demand and surplus generation events. This method was applied to 40 years of historical (1979-2018) meteorological data taken from the ERA5 meteorological reanalysis dataset (Hersbach et al., 2018), and the resulting adverse weather events within the historical report were presented.

Since these adverse weather events occur when electricity generation and demand are high or low, methods for estimating electricity generation and demand from weather data were first developed. These representations of electricity generation and demand were then used to quantify unfavourable conditions through adverse weather metrics. In doing so, this approach draws on insights from the electricity modelling literature, such as Bloomfield et al. (2019), hydrological drought modelling literature, such as Burke et al. (2010), and the expertise of the project advisory and user groups.

Below is a brief overview of the steps in the Phase 2 (a) approach is to give context for the application of some methods in Phase 3 (a), as presented in full in Section 3. Please refer back to the Phase 2 (a) report for further detail on the method development (Dawkins and Rushby, 2021).

Steps in the Phase 2 (a) approach:

1. Estimate regional weather dependent electricity demand (WDD) from air temperature as a function of heating degree days (HDD) and cooling degree days (CDD).
2. Estimate regional daily wind generation using 100m wind speed data, the potential location of wind turbines and a weighting of installed capacity. The wind speed data was bias corrected using the Global Wind Atlas⁴.
3. Estimate regional solar generation using air temperature and incoming surface solar radiation, the potential location of solar panels and a weighting of installed capacity.
4. Calculate the Wind-Drought-Peak-Demand Index (WDI) – a stress event index relating to the daily Demand-Net-of-Renewables. These events occur within a region when wind speed is low, leading to low renewable electricity generation, and when there is a high demand, for example in the winter and summer when there is higher demand for heating and cooling, respectively.

⁴ <https://globalwindatlas.info/> (Accessed 22/09/2021)

5. Calculate the Surplus-Generation-Index (SGI) – a stress event index relating to the daily Renewables-Net-of-Demand. These events occur within a region when wind speed and solar radiation are high, leading to high renewable electricity generation; and temperatures are moderate to high/low, leading to low heating/cooling demand in winter/summer.
6. Identify long-duration adverse weather stress events (when the WDI and SGI exceed its 90th percentile) in the historical observations period and characterise these events in terms of severity and duration.
7. Undertake a sensitivity study to assess the sensitivity of assumptions around the demand model, turbine power curve, installed capacity and accumulation period within the index definitions and the adverse weather stress events that are identified.

Phase 2(b): Developing the dataset of long-duration events

2.2 Phase 2b builds on the previous work by identifying adverse weather stress events in two further data sources: historical climate model hindcasts (providing more than 2000 alternative plausible weather years) and future climate projections (capturing how weather is likely to change in future climates). The methods developed for calibrating and imputing these climate model data sources are presented in Dawkins et al. (2021b). The three data sources (historical observations from phase 2a and climate model data from phase 2b) are then used in combination to quantify the extremity (i.e. the return period) of long-duration adverse weather stress events, and how these may change in future warmer climates. This information is subsequently used to select relevant events for the final dataset.

The resulting dataset characterises long-duration winter-time and summer-time wind-drought-peak-demand events and summer-time surplus-generation events in the UK and in Europe. It contains gridded daily average meteorological data (surface temperature, 100m wind speed and surface solar radiation) associated with a range of examples of such events, capturing various extreme levels (1 in 2, 5, 10, 20, 50 and 100 year return period events) and climate warming levels (current day, 1.5°C, 2°C, 3°C and 4°C above pre-industrial levels). The dataset is freely available to download from the CEDA archive⁵ (Dawkins et al., 2021a).

⁵ <https://catalogue.ceda.ac.uk/uuid/7beeed0bc7fa41feb10be22ee9d10f00> (Accessed: 19th August 2021)

3 Characterising short-duration ramping events

This section will present the methods used to characterise short-duration ramping events associated with wind and solar renewable energy. The approach draws on the previous methods developed in Phase 2 of the project in combination with those explored in Cannon et al. (2015). A wind ramping event is characterised by large changes in wind speed, and subsequent wind power production, during a short time window, whilst a solar ramping event is characterised by large instantaneous fluctuation in solar irradiance (solar radiation reaching the surface) impacting on solar power production. Both ramping events are characterised by rapid change in a meteorological variable that impacts the capacity factor of a renewable energy system, and subsequently electricity generation.

The capacity factor defines, for a given time period, the ratio of actual generation compared to the maximum potential generation. When the wind speed is slower, or the amount of solar radiation reaching the surface decreases, the capacity factor decreases i.e. there is a reduction in the potential for generation. The capacity factor can also be impacted by other meteorological variables, for example, solar capacity factor is also a function of air temperature, or in the case of wind generation, the capacity factor is impacted by the choice of wind turbine and its associated power curve. Whilst a ramping event can be identified by a rapid change in *generation*, it is possible to use the change in *capacity factor* to represent the generation change. This is because these quantities are proportional to each other (generation = capacity factor x installed renewable capacity). Similar to Cannon et al. (2015), this phase will use changes in capacity factor to characterise short-duration adverse weather stress events (i.e. ramping events) and then identify such wind and solar ramping events for the

3.1 historical period 1979-2014 in Great Britain.

Estimating wind electricity capacity factor

The method for estimating hourly wind electricity capacity factor detailed below follows the same approach used in phase 2 and similarly is based on a number of insights from Bloomfield et al. (2019). The calculation is based on gridded wind speed data, specifically Euro4⁶ hindcast model level 5 wind speed data. This model level provides the wind u and v vector components at 93m above the terrain, which are combined to calculate wind speed in each grid cell, and is the closest representation from the model of 100m wind speed data (i.e. wind speed 100m above ground level), thought to be representative of the wind at turbine height. It is possible to interpolate the data between model levels to obtain wind speed at precisely 100m at any

⁶

https://www.metoffice.gov.uk/binaries/content/assets/metofficegovuk/pdf/data/european_model_data_sheet_lores1.pdf (Accessed: 19th August)

given grid point, but these methods are complex and computationally expensive. Additionally, the calibration of the Euro4 data, detailed below, performs a similar process whilst simultaneously removing bias within the wind speed data itself. Therefore, for the purpose of this report, the wind speed calculated from the Euro4 model level 5 wind vector component data will hereafter be called 100m wind speed data.

There are known substantial biases that exist in the ERA reanalysis datasets and therefore, similar to phase 2 and in line with Bloomfield et al. (2019), the Euro4 hindcast data is bias corrected using the New European Wind Atlas (NEWA) project data⁷, a wind-resource assessment dataset at a 3km resolution. This dataset was chosen over the Global Wind Atlas (used in phase 2) due to being the latest product available. An additional benefit was the availability of the NEWA data at a similar resolution to Euro4, resulting in a more accurate transformation process and therefore bias correction. The NEWA data was transformed to match the Euro4 grid and the monthly mean and standard deviation calculated for each grid cell for the bias correction. Similar to phase 2 of the project, the Euro4 wind speed data was bias corrected using a normal variance scaling method on a grid-point by grid-point basis (i.e. correcting each grid point separately), using the NEWA wind speed data interpolated to each grid cell as the 'truth'. As in phase 2a, only the reanalysis wind speed data is bias corrected (the solar radiation and temperature data used in the solar capacity factor calculation is not adjusted).

Euro4 is a hindcast dataset, produced by dynamically downscaling the ERA-interim reanalysis dataset. In order to align the downscaled data with the data it is derived from, the Euro4 model is reinitialised at regular intervals, preventing it from deviating freely from what is known to have occurred. This means that there is a daily discontinuity as the hindcast switches from one model run to the next. For most usages, these changes are not generally noticeable, but when analysing the short term (hour to hour) changes in wind speed they become more apparent. This leads to many of the largest changes to wind speed (and hence 'changes in capacity factor', defined below) identified from the Euro4 record, in fact occurring as a result of the model reinitialisation as opposed to any meteorological conditions which could occur in practice, and must be accounted for as described in Section 3.3.

For every hour on a given day, the wind power capacity factor, defined as the proportion of a turbine's maximum possible generation produced, is calculated for each grid cell separately by applying the turbine power curve to the bias corrected 100 m wind speed. The same three on-shore wind turbine power curves used by Bloomfield et al. (2019) and phase 2 of this

⁷ <https://map.neweuropeanwindatlas.eu/about> (Accessed: 19th August)

project have been used to calculate the capacity factor in a given grid cell. These 3 turbines were chosen by Bloomfield et al. (2019) to be representative of type 1, 2 and 3 turbines from the International Electrotechnical Commission (IEC) wind speed classification respectively (IEC, 2005). In each land grid cell, the most appropriate turbine (out of these three options) is chosen, based on the average weather conditions there. Specifically, as in Bloomfield et al. (2019), it is assumed that all of the turbines within a grid cell are of the same type, and the selected turbine type is the one that maximises the capacity factor for the 36-year (1979-2014) mean of the bias corrected 100 m wind speed in that grid cell. Following the continued guidance from the project advisory group, the off-shore wind power capacity factor is specified as following the power curve used by National Grid when modelling off-shore turbines (described in Section 3.2 of nationalgridESO 2019).

Within each grid cell, the wind power capacity factor is then weighted by the potential for installed wind capacity within that grid cell. The potential for installed wind capacity is based on the analysis of Price et al. (2018), Moore et al. (2018) and Price et al. (2020). Within these studies, the potential locations of on-and offshore wind turbines in Great Britain are derived based on in-depth explorations of technical, social and environmental restrictions. For example, on-shore restrictions include terrain steepness, distance from housing and the location of nature conservation areas, while off-shore restrictions include water depth, shipping routes and the UK government approval of off-shore regions for energy production.

The weighted wind power capacity factors are then aggregated into the defined project regions for onshore (Figure 1a) and offshore wind (Figure 1b). For onshore wind there are three regions: Scotland (blue), East England (green) and West England and Wales (red), which were defined based on the long-term climatology of mean annual 100m wind speed across the region, calculated from the NEWA data. These are referred to within this report as 'Onshore North', 'Onshore East' and 'Onshore West'. Offshore wind has been handled independently of onshore wind and separated into a north (orange) and south (purple) region following insights from the project advisory group.

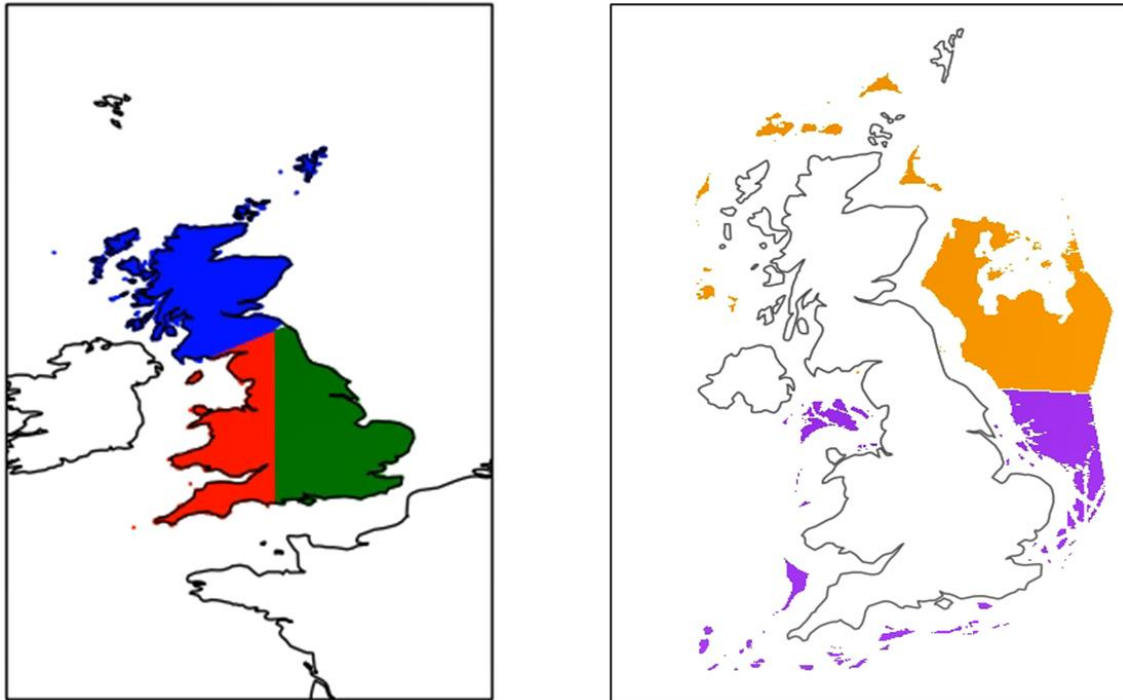


Figure 1: (a - Left) Defined project regions for Onshore wind: Scotland (blue), East England (green) and West England and Wales (red), and (b - Right) Defined project regions for offshore wind: offshore north (orange) and offshore south (purple).

In summary, the hourly wind power capacity factor in a region is found by multiplying the wind power capacity factor, in each grid cell within that region, by the potential installed wind capacity weighting calculated for that grid cell (as a fraction of the total capacity weight in that region) and aggregating over the region.

To validate the resulting data, daily means of wind power capacity factor for Great Britain were calculated for each year and plotted against the daily mean of wind power capacity factor for United Kingdom that were calculated using ERA5 data in phase 2 (Dawkins et al. 2021b). This validation (Appendix 2) shows good agreement between the datasets across the years. Note minor discrepancy between the means is expected due to the phase 2 results including results for Northern Ireland, and small differences in the underlying meteorological data. This confirms that the hourly wind capacity factors have been calculated successfully in this phase of the project.

3.2 Estimating solar electricity capacity factor

The method below, as per phase 2, is based on insights from Bloomfield et al. (2019), who follow a similar approach to Bett and Thornton (2016). Similar to Bloomfield et al. (2019), the calculation is based on gridded near surface air temperature and incoming surface solar radiation over land. As in the previous sections of this report, these variables are taken from the Euro4 hindcast dataset.

On a given day and within a given land grid cell, the solar power capacity factor, defined as the proportion of a solar panel's maximum possible generation produced, is calculated based on a linear function of the surface temperature and incoming surface solar radiation. This function first calculates the relative efficiency of the solar panel, η , as a function of surface temperature at that location and time, T :

$$\eta(T) = \eta_r(1 - \beta_r(T - T_r)) \quad (1)$$

where η_r is the photovoltaic panel efficiency evaluated at the reference temperature T_r , and β_r is the fractional decrease of cell efficiency per unit temperature increase. Following Bloomfield et al. (2019) and Bett and Thornton (2016), the constants in Equation 1 are defined as: $\eta_r=0.9$, $T_r=25^\circ\text{C}$ and $\beta_r=0.00042$. Here, the temperature at the location of the solar panel, T , is the grid cell near surface temperature value taken from the ERA5 dataset. The solar power capacity factor at the given time and location (grid cell) is then calculated as:

$$\text{CF} = \eta(T) \frac{G}{G_r} \quad (2)$$

where G is the incoming surface solar radiation at that location and time, and G_r is the reference incoming surface solar radiation, set to 1000Wm^{-2} as in Bloomfield et al. (2019). As these are linear functions of temperature and solar radiation, solar generation varies linearly with these meteorological variables. This linear relationship is increasing with solar radiation and decreasing with temperature.

As in Section 3.1, the solar power capacity factor within each grid cell is then weighted by the potential for installed solar capacity within that grid cell. The potential for installed wind capacity is based on the analysis of Price et al. (2018) and as for installed wind capacity, Price et al. (2018) devise a region within Great Britain, within which solar capacity could be installed, based on a number of technical, social and environmental restrictions. These include ground steepness, land use type (e.g. areas of outstanding natural beauty), and policies to protect wildlife habitats.

The weighted solar power capacity factors are aggregated into the defined project regions (Figure 2), of which there are three: Scotland (blue), North England (red) and South England and Wales (green). The regions for solar differ from those used in the onshore wind analysis as incoming solar radiation has a stronger correlation with latitude rather than longitude, therefore an east/west split would be of little additional value. As in described in Section 3.1, the aggregated weighted solar power capacity factors are then scaled by the total region area capacity to obtain the final hourly solar capacity factor in each region.



Figure 2: Defined project regions for solar: Scotland (blue), North England (red) and South England and Wales (green).

As described in Section 3.1, a validation was undertaken for each year to compare the daily means of solar power capacity factor for Great Britain against the daily mean of solar power capacity factor for United Kingdom calculated using ERA5 data in phase 2. Similarly, the 3.3 validation indicated a good agreement between the datasets (Appendix 2).

Calculating the change in capacity factor over time windows

Using the methods described in Section 3.1 and 3.2, we are able to produce a time series of hourly capacity factor from 1979-2014 for Great Britain and our defined wind and solar regions. As in Cannon et al. (2015), a short-duration ramping event for a given region, is quantified as the maximum change in capacity factor, within a given time window. The time windows explored are those used by Cannon et al. (2015): 1 hour, 3 hours, 6 hours, 12 hours and 24 hours. For a given time window e.g., 3 hours and region e.g. Scotland, the number of times this 'maximum capacity factor change' surpasses a particular change threshold can be calculated. As in Cannon et al. (2015), the average number of ramping events per year that surpass each change threshold of interest for a given time window can then be determined. This allows us to compare our analysis of ramping events to that of Cannon et al. (2015), and provides insights into the frequency of different size ramping events in any suitable meteorological dataset.

An important thing to note is this calculation is carried out using rolling time windows, moving through the hourly timeseries data from 1979-2014. The maximum change in capacity factor could occur at any point during a given time window, and therefore where two-time windows may overlap, there is the potential for repeated data points where one ramping event is double counted. For example, as shown in Figure 3 below, these two 3-hour time windows (indicated in black) have the same maximum change in capacity factor but are counted as two ramping events. The repeated data points will need to be handled during the extreme value analysis (EVA).



Figure 3: Schematic to show two overlapping 3-hour time windows (black) over a timeseries (pink) which would have the same maximum change in capacity factor.

In addition as mentioned in Section 3.1 the reinitialisation of the model underlying the wind speed data may result in spurious ramps being identified. For this reason, if a 1, 2 or 3 hour window contains such a model reinitialisation, then it is excluded from the further analysis so that conclusions are based upon plausible meteorological conditions rather than model features. For longer time windows the reinitialisation was found to not make material difference to the ramps identified.

3.4 Finally, as described in Section 3, the capacity factor defines, for a given time period, the ratio of actual generation compared to the maximum potential generation. As a ratio, the capacity factor is unitless and is usually given as a number between 0 and 1. For the presentation of results in this report, the capacity factor is given as a number between 0 and 100 to allow for the replication and comparison of analysis carried out in Cannon et al. (2015). This should not be confused as a percentage change in capacity factor. For example, within this report, a change in capacity factor of 50 is equivalent to an absolute change of 0.5 (i.e. a capacity factor dropping from 0.8 to 0.3), **not** a 50% change (e.g. a capacity factor decrease from 0.8 to 0.4).

Extreme Value Analysis

For each time window and region, an empirical EVA is carried out to contextualise the extremity of ramping events, particularly focusing on the most extreme events. This empirical (i.e., based on the observed data record only) EVA identifies the observed *return period* (number of years in between events) of ramping events of a given *return level* (extremity of

'change in CF'). For example, allowing us to identify that, for wind ramping events in 3-hour time-windows in the Onshore North region, a change in CF of 70 occurs on average once every 10 years.

For each time window and region, the empirical return period (in years) of each ramp 'event' (i.e., the maximum change in CF in each overlapping time window) is estimated empirically by firstly ranking all events in ascending order, equivalent to calculating the event percentile. This calculates the event frequency in terms of events, for example, as described in phase 2a (Dawkins and Rushby 2021), the 50th percentile event (ranked exactly in the middle) is the event expected to occur once every 2 events. These percentiles are then scaled by the number of years and the number of events in the data record, to give a return period in terms of years (rather than events). For example, we have **36 years** of data (1979-2014) and there are 315,549 overlapping 3-hour time windows in 36 years (i.e. **315,549 events**), hence the 1 in 2 events 3-hour time window event (the 50th percentile or middle ranked) is the 1 in $36 / (0.5 \times 315,549)$ year event (i.e., the 1 in 0.0023-year event, hence expected to occur 4382 times per year). Similarly, here, the 99.99th percentile event is the $36 / (0.0001 \times 315,549)$ year event (i.e. the 1 in 1.14-year event, hence expected to occur approximately once per year).

As noted in Section 3.3, the way in which the ramping events are characterised leads to some events being double counted, and hence the events being temporally correlated. This can lead to a misrepresentation of the return period of events (Coles, 2001). To overcome this, the events are 'de-clustered' before the return periods are estimated using the approach described above. De-clustering is achieved by firstly defining a high threshold, then each time this high threshold is exceeded for multiple events in a row, only the most extreme event is retained. This ensures the same ramping event is not represented multiple times within the extremes of the dataset, and hence the EVA. Here, the data for each time window and region is de-clustered using a 95th percentile threshold.

This method is used to identify the 1 in 2, 5, 10, 20 and 30-year return period wind and solar ramping events for each region and time window combination. This allows for return level curves to be plotted for each region and time window, for comparison. Examples of such events are also selected from the Euro4 data record, presented in tables, and as timeseries plots for context (see Sections 4.1.3 and 4.2.2).

4 Results

Wind

In this section we present the analysis of historical observed wind ramping events from the Euro4 data record. This analysis follows closely with the approach taken by Cannon et al. (2015), with equivalent plots produced. Firstly, this is done for GB as a whole for comparison with Cannon et al. (2015), and secondly for each of the 5 wind regions separately.

4.1.1 Maximum change in capacity factor in Great Britain over various time windows

Figure 4, equivalent to Figure 9(c) in Cannon et al. (2015), shows, for a given time window on the x-axis, the number of times in an average year that the maximum change in capacity factor (hereafter referred to as ΔCF) surpasses a particular change threshold (y-axis) in Great Britain. For example, in an average year, the maximum change in capacity factor during a 6-hour time window will surpass at least 10 between 4000–8767 hours per year compared to surpassing at least 47 between 10-100 hours per year. The most extreme ramping event identified in Great Britain across the 36-year time series (indicated by the dashed line) during a 6-hour time window was a ΔCF of 68.

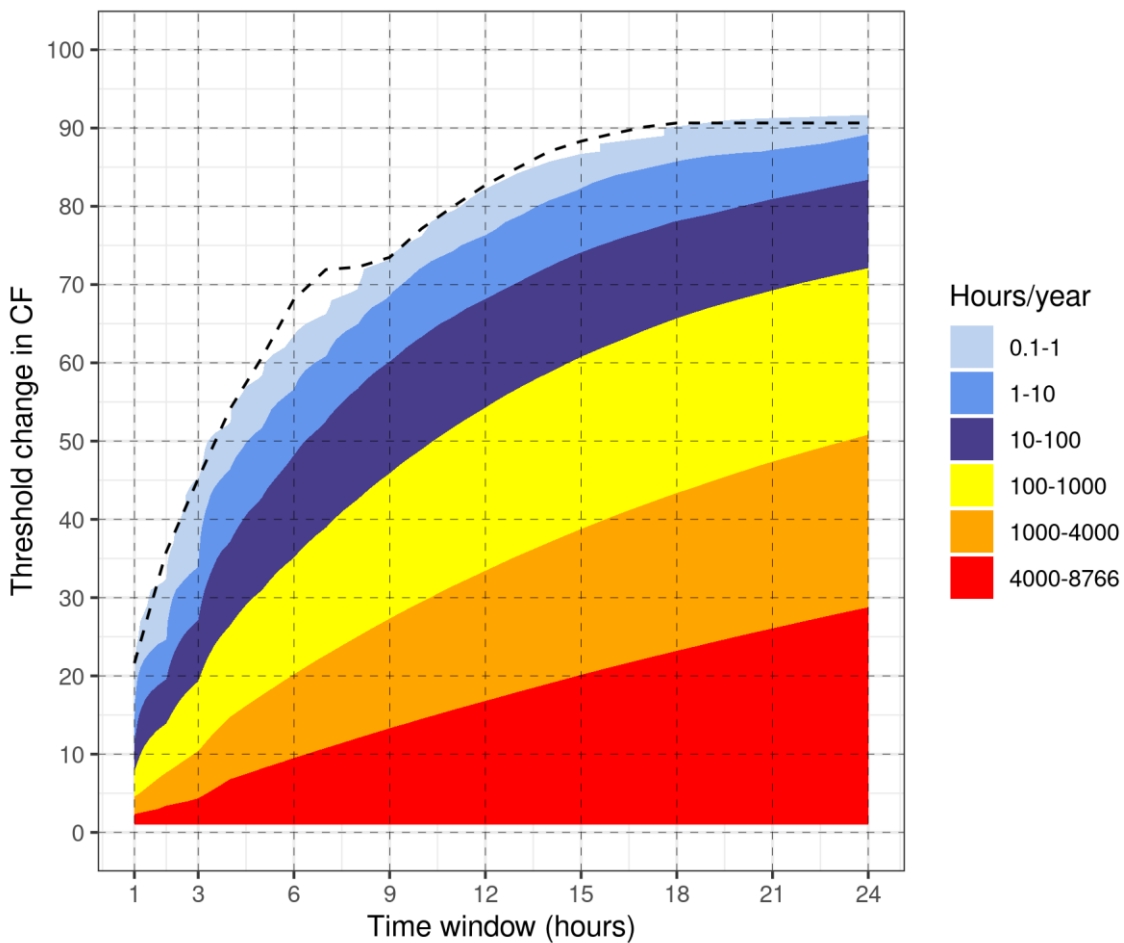


Figure 4: The frequency of hours, in an average year, for which there is a subsequent ramp in generation of at least ΔCF (y-axis) within the given time window (x-axis) for Great Britain. The dashed lines mark the most extreme events in the 36-year time series (1979-2014). ΔCF = maximum change in capacity factor observed in a given time window.

Cannon et al. (2015), from which this method was based on, explored the frequency of rapid change wind ramping events in the UK from 1980-2012 and noted the following key observations:

- As the threshold change increases or the time window decreases, the definition of a ramp becomes more stringent and therefore ramping becomes rarer.
- In correspondence to the transition time of a typical low pressure (cyclonic) weather system over the UK, the most extreme changes in maximum capacity factor change (indicated by the dashed line) increases rapidly with the time window up to around 9-12 hours, after which it plateaus.

The results presented are consistent with those produced by Cannon et al. (2015) and the observations outlined above, although the observed changes in capacity factor are generally 10% higher here. This is hypothesised to be due to the difference in the wind power curves

used, with the power curve in the Cannon et al. (2015) paper plateauing at a 90% capacity factor, and the different spatial distribution of wind turbines across Great Britain.

Cannon et al. (2015) found that the most extreme changes in capacity factor (the dashed line) increase rapidly with time window to around 12 hours, after which it plateaus. They associate this with the transition time of a typical low pressure (cyclonic) weather system over the UK. Figure 4 shows a more gradual increase in the most extreme changes in capacity factor with time window in comparison to Cannon et al. (2015), with a later plateau at closer to 15 hours. It is suspected that this difference is largely reflecting the difference in region size over which the capacity factor is aggregated, with this work undertaken over a wider GB domain, capturing more offshore wind regions. Therefore, the transition time of weather system across GB is expected to take longer to move across the larger domain. Furthermore, it is also anticipated that the increased spatial resolution of the Euro4 hindcast meteorological data is more accurately representing the meteorological extremes in the shorter time windows, compared to MERRA reanalysis data (50km) used in Cannon et al. (2015), and could explain the additional variability captured in the most extreme changes in capacity factor.

4.1.2 Maximum change in capacity factor across defined regions over various time windows

Figure 5, equivalent to Figure 9(c) in Cannon et al. (2015), shows, for a given time window on the x-axis, the number of times in an average year that the maximum change in capacity factor change (ΔCF) surpasses a particular change threshold (y-axis) for each of the defined regions for onshore and offshore wind. Looking at 'Offshore South' as an example (Figure 5, third row, left), the most extreme ΔCF observed in a 1-hour time window in the last 36 years is 42 (black star). For the same region, in an average year, the ΔCF surpassing at least 28 was observed less than once a year during a 1-hour time window compared to between 4000-8766 times during a 24-hour period.

There are some subtle differences in the regional plots shown in Figure 5. For example, 'Onshore East' frequently experiences larger ΔCF during the shorter time windows, indicated by the steep gradient of the dashed line between the 1–6-hour time windows - the maximum ΔCF seen in a 6-hour time window is approximately the same as that of a 24-hour window. In terms of wind ramping events observed over the 36-year timeseries, 'Onshore East' reaches the plateau of threshold change by the 6-hour time window, in comparison to the 9-hour time-window for 'Onshore North' and 'Onshore West'. In an average year, both offshore regions are observed to have smaller, less frequent ramps during the shorter time windows compared to the onshore regions, indicated by the gentler increasing slope of the dashed line through

the time-windows. Further, of all the regions, 'Offshore North' has the smallest observed maximum change in capacity factor ($\Delta CF = 33$) during a 1-hour time window across the 36-year timeseries.

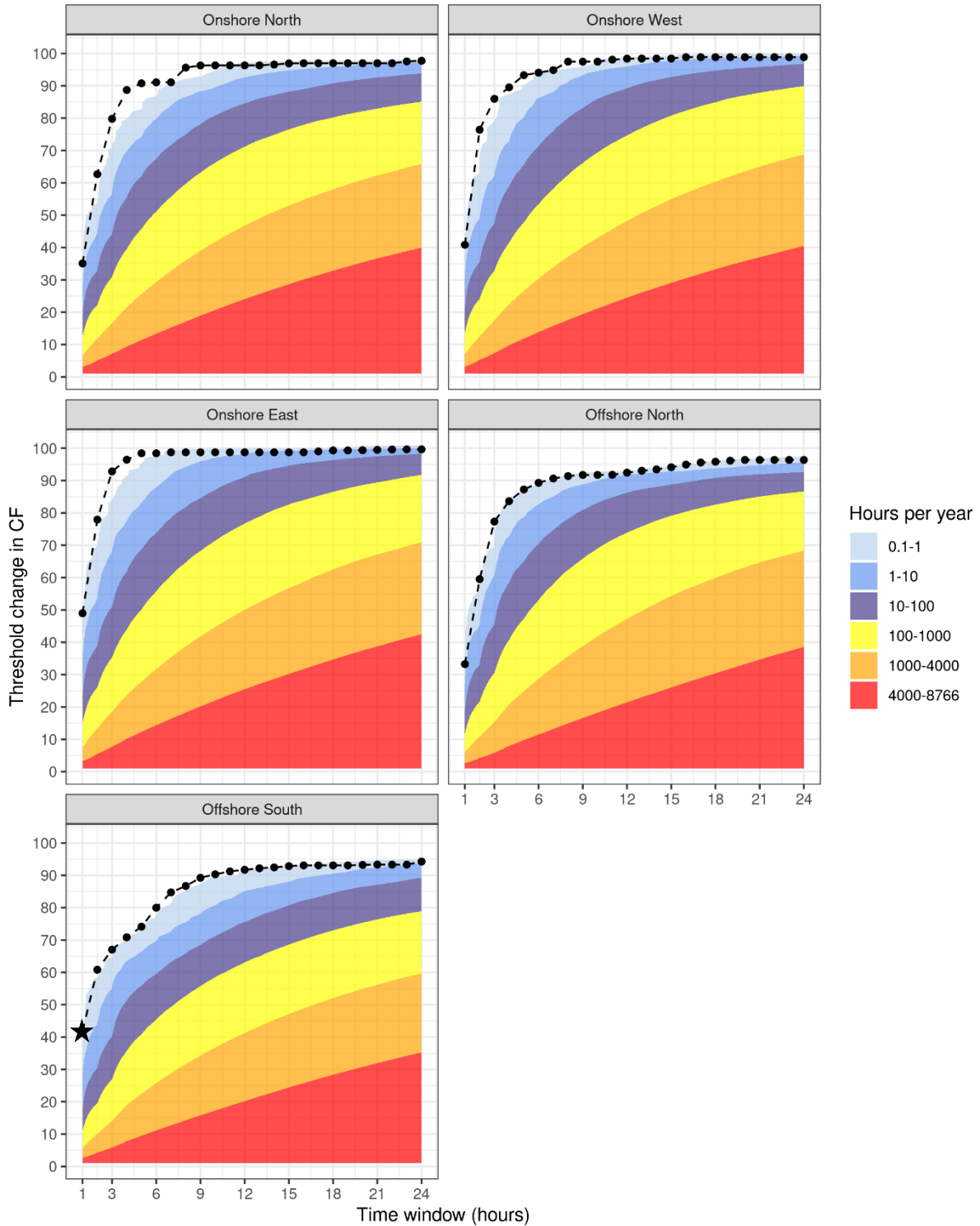


Figure 5: The frequency of hours for which there is a subsequent ramp in generation of at least ΔCF (y-axis) within the given time window (x-axis) for the defined regions of onshore and offshore wind. The dashed lines mark the most extreme events in the 36-year time series (1979-2014).

Figure 6, equivalent to Figure 8(c) and (f) in Cannon et al. (2015) shows, for each region (one per row) and time window (coloured lines), the number of times in an average year (y-axis) that a ramp event is observed reaching or exceeding a threshold of ΔCF (x-axis). Each line on the plot represents a different time window (1-, 3-, 6-, 12- and 24- hour time windows) with a row per a defined region – identified in the top grey bar. The right-hand panel presents an exploration of the less frequent ramping events for each region i.e., focusing on events reaching a threshold change less than 150 times (number of hours) in an average year. For example, in the case of ‘Onshore North’, Figure 5 indicates that, in an average year, the maximum change in capacity factor surpassing at least 40 was observed between 10-100 times during a 3-hour time window. The left-hand panel of Figure 6 below suggests that, for the same region and time window there is a plateau towards 0 occurrences for all threshold changes above $\Delta CF = 25$. Using the right-hand panel of Figure 6, it is possible to explore these lower frequency events in higher resolution and read from the plot that, during an average year, $\Delta CF \geq 40$ in a 3-hour window occurs approximately 20 times in the ‘Onshore North’ region (highlighted by the red star).

Figure 6 highlights that, in an average year, the number of times a ramp reaches a threshold of capacity factor change decreases as that threshold increases i.e., the higher thresholds are surpassed less often. A common feature across all the regions is that the maximum change in capacity factor (ΔCF) is larger during the bigger time windows, which is consistent with the findings of Cannon et al. (2015). This is particularly evident when focusing on the less frequent ramp events occurring in an average year, highlighted in the right-hand panel of Figure 6. Comparing the 1-, 6- and 24-hour time windows for ‘Onshore West’, the threshold for maximum change in capacity factor observed around 125 times in an average year, is around 15, 50 and 90, respectively. As a similar observation can be made across all of the regions, the national electricity system may be vulnerable should these larger changes occur simultaneously within the longer time window. Hence, to allow energy modellers to explore this potential vulnerability, the final data set of short duration events will contain spatial fields of meteorological data covering all of GB and the offshore region for the full time slice of the passage of weather systems.

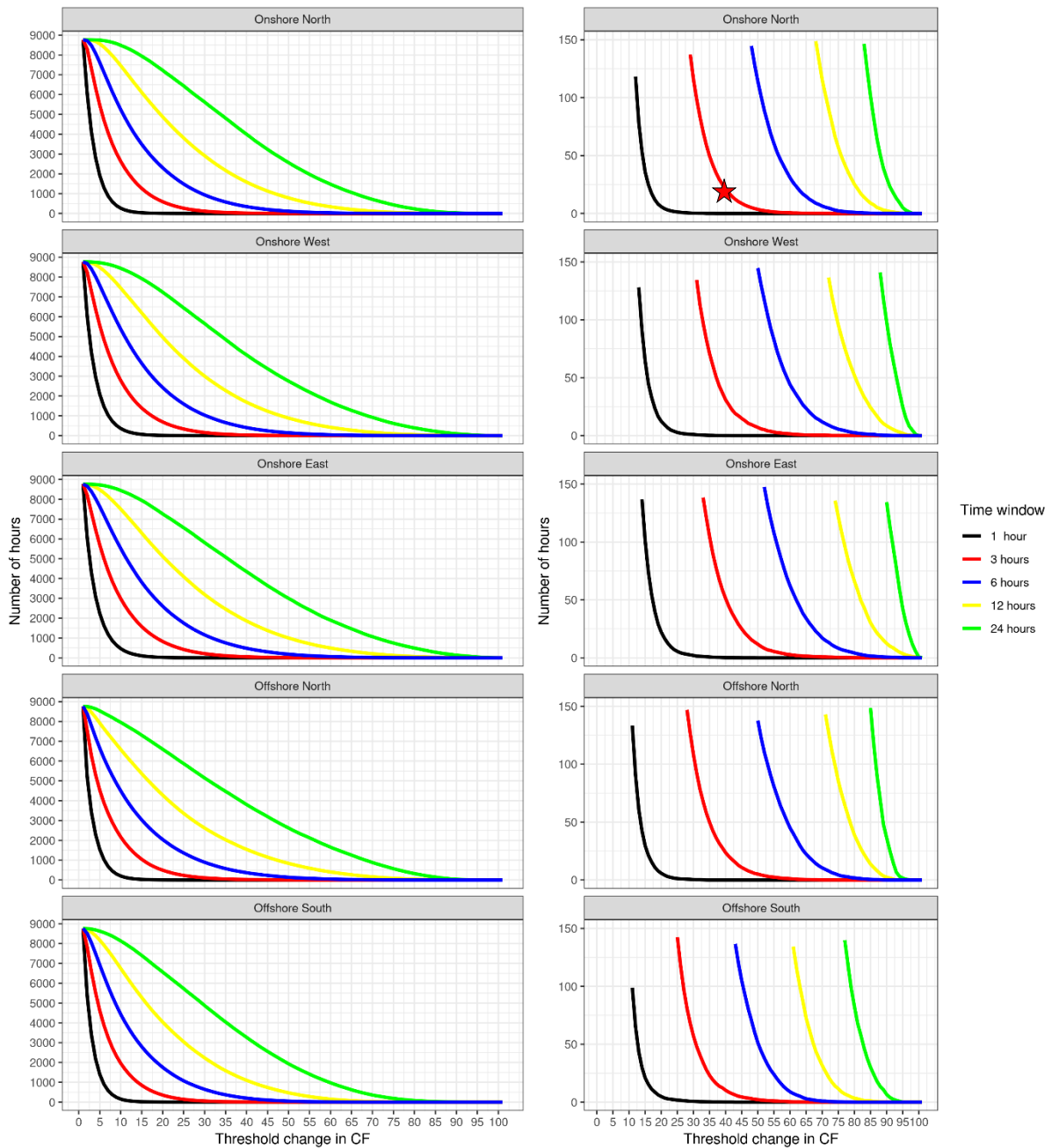


Figure 6: The number of hours in an average year (y-axis) that a ramp event is observed reaching or exceeding a threshold of ΔCF (x-axis). Each line on the plot represents a different time window (1-, 3-, 6-, 12- and 24- hour time windows) with a row per a defined region – identified in the top grey bar. The right-hand panel presents an exploration of the less frequent ramping events for each region i.e., focusing on events reaching a threshold change less than 150 times (number of hours) in an average year.

Similarly, Figure 7 shows, for each time window (one per row) and region (coloured lines), the number of times in an average year (y-axis) that a ramp event reaches or exceeds a threshold of capacity factor change (x-axis). The uniform shape of the different coloured lines indicate that the different regions are relatively consistent in their fluctuations of ΔCF across the various time windows. There is also a slight indication that the two offshore regions have a smaller magnitude in fluctuations compared to onshore regions, particularly offshore south, indicated

by the leftward shift of the pink lines in Figure 7. It is hypothesised that the offshore regions experience smaller fluctuations as a result of the greater spatial distribution of turbines over a wider area, in comparison to the onshore regions. This means that as a low-pressure weather system moves across, it is less likely for the whole region to be disrupted simultaneously, with non-affected areas balancing those experiencing fluctuations (in the sense of averaging the capacity factor change over the region). Of the two offshore regions, Offshore South is the most widely distributed, with turbine capacity spanning off the east and west coasts of southern England. Furthermore, when observing the capacity factor maps (not shown here), the overall capacity of Offshore South is less, which means theoretically there is less potential magnitude for change to start with. These findings, whilst not taking account of the flexibility offered by storage, or other implications governing turbine locations, support the results of Drew et al. (2017) that favour an increased spatial distribution across Great Britain, both onshore and offshore, to improve energy system resilience.

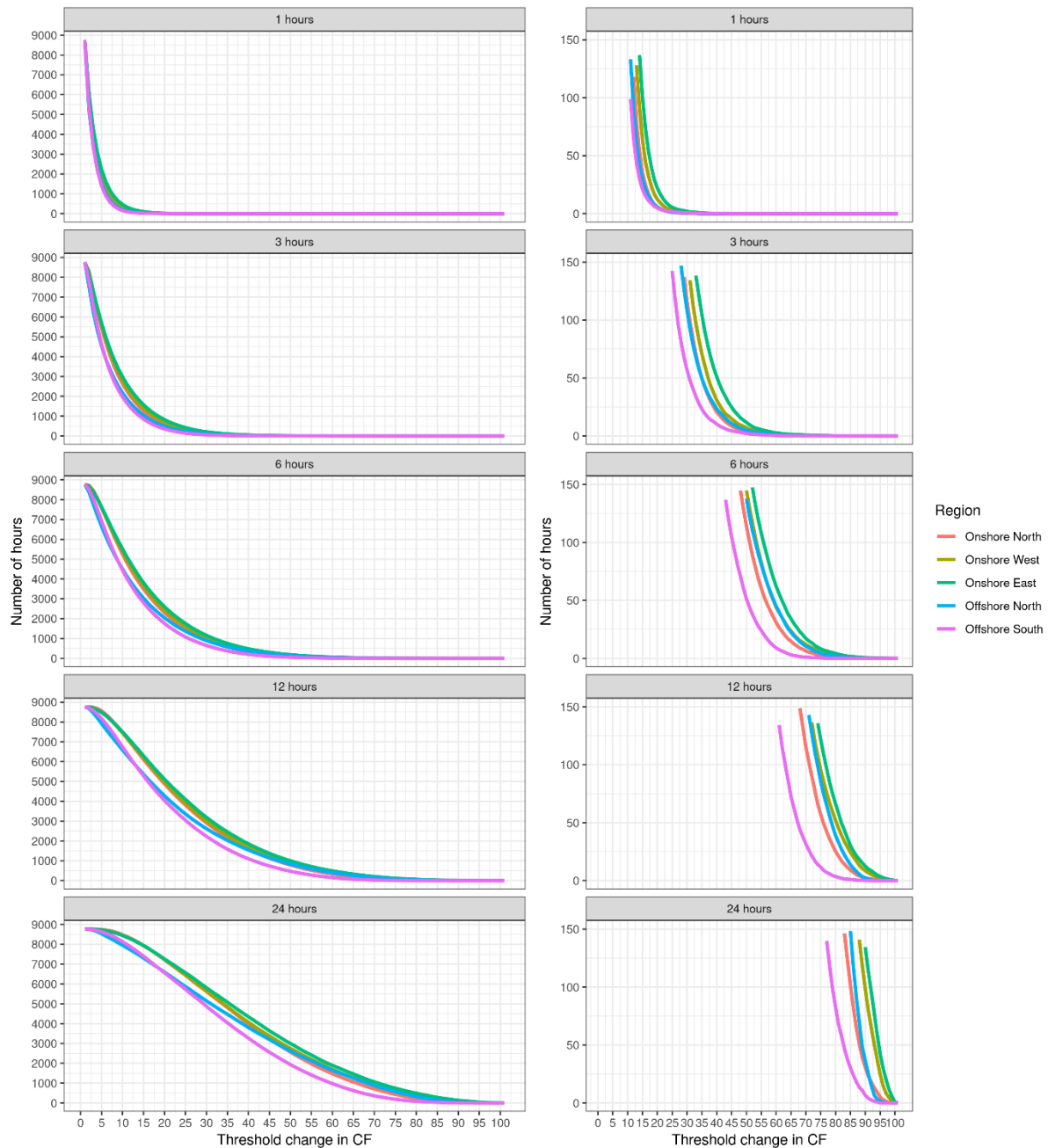


Figure 7: The number of hours in an average year (y-axis) that a ramp event is observed reaching or exceeding a threshold of ΔCF (x-axis). Each line on the plot represents a different defined region with a row per a time window – identified in the top grey bar. The right-hand panel presents an exploration of the less frequent ramping events for each time window i.e., focusing on events reaching a threshold change less than 150 times (number of hours) in an average year.

Plots to explore the interannual and seasonal variability of wind ramping events in an average year (equivalent to Figure 11 and 12 (c) and (f) in Cannon et al. (2015)) were also produced for the different regions, and are Appendix 3 and 4, respectively.

Cannon et al. (2015) observe large interannual variability, which is particularly true for the most extreme events. Whilst the full range plot in the left-hand panel of Appendix 3 appears to present little year-to-year variability for any time window or region, the right-hand panel

presenting the least frequent events does highlight a greater magnitude of variability in the most extreme events, as observed in Cannon et al. (2015). Onshore East and Onshore West appear to have the most variability of the regions, particularly so in the most extreme events observed in any one year where thresholds changes in capacity factor are surpassed less than 100 hours per year. The deviation away from the mean is greatest in events observed less than 50 times, which is a common feature across the regions, although to varying magnitudes. A consideration for the resilience of future systems may be that even small differences in the observed year-to-year variability (i.e., a small number of extreme ramping events with ΔCF that deviate from the mean) could multiply up in significance if there is an increased capacity of wind installed.

Appendix 4 shows that the most frequent but small ΔCF appear to occur most often in summer and spring with these seasonal lines falling above the average season and autumn and winter falling on or below, which holds across the regions for ΔCF up to between 20-30. Cannon et al. (2015) note that the mean frequency of ramps varies seasonally, noting that there are many more extreme ramps in winter than in summer, likely due to the cyclonic activity over the UK in winter. This is consistent with the findings observed in the right-hand panel of Appendix 4, although observed to a lesser extent in the 'Onshore North' (Scotland) region where there is little seasonal variability, indicated by the overlapping of the different season lines and minimal deviation from the average season. This could probably be related to orographic impact on wind, that means wind speed volatility and variability is greater across land in Scotland in the summer compared to the southern regions which have less highland areas proportional to the region size. The seasonal variability for 'Offshore South' tightens (i.e., less difference between seasons) as ΔCF surpasses the 80 threshold. Comparatively, the seasonal distribution of 'Offshore North', 'Onshore East' and 'Onshore West' narrows closer towards the least frequent events, surpassing the 90 threshold of change. Interestingly, Cannon et al. (2015) observe little seasonal variability between summer and winter in the very most extreme ΔCF events for Great Britain, which appears to be true for this analysis also.

4.1.3 Return periods and return levels of extreme events

Figure 8 presents the results of the empirical extreme value analysis, carried out to calculate the *return period* ('expected' number of years in between events) of wind ramping events of a given *return level* (extremity of 'change in CF'). The left-hand panel presents the return period (x-axis) and return level (y-axis) for a time window (each coloured line) within a defined region (each plot). For example, in the 'Offshore South' region, a 1 in 10-year event has a return level

(ΔCF) of 40 in a 1-hour time window (black star) and 77 in a 6-hour time window (blue star). Conversely, the right-hand panel presents the return period (x-axis) and return level (y-axis) for a defined region (each coloured line) within a given time window (each plot). For example, for a 1 in 30-year event in a 3-hour time window, 'Onshore North' observed a return level of 77 (orange star) whilst 'Onshore East' observed a return level of 90 (green star).

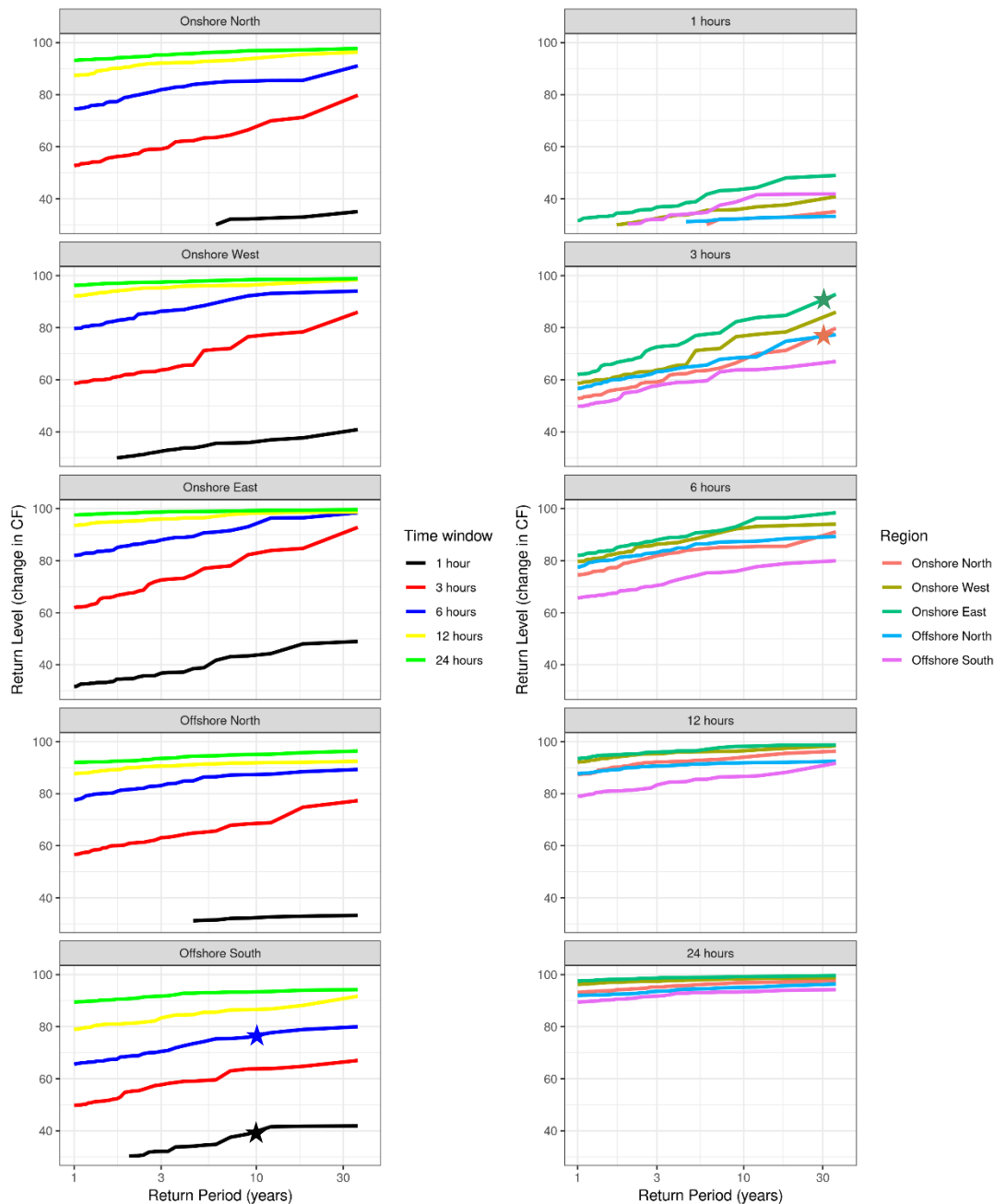


Figure 8: The return period (number of years in between events, x-axis) of wind ramping events of a given return level (extremity of 'change in CF', y-axis) for each time window and region combination. The left-hand panel presents each time window within a defined region. Conversely, the right-hand panel presents each defined region within a given time window.

Table 1 provides a selection of example events for different time windows and return periods observed in the Euro4 hindcast dataset for 'Onshore West'. Equivalent tables are available for the other regions in Appendix 5-8. The table shows for each event in a given time-window, the return period, return level and a date/time for the end of the window in which the event occurred. For example, the event in row 20⁸ is an example of a 1 in 2-year event in a 12-hour time window that occurred between 3pm 5th December 2001 and 3am 6th December 2001, with the latter date/time presented in the final table column. This event had a return level of 94.54.

Table 1: Example wind ramping events observed in the Euro4 hindcast dataset in 'Onshore West' for different time windows and return periods. The first column indicates the length of the time-window in which an event was observed. The second column indicates the return period i.e., number of years in between events. The third column indicates the observed return level (extremity of 'change in CF'). The fourth column indicates the date/time for the end of the window in which the event occurred.

	Time window (hours)	Return period (years)	Return level (change in CF)	Date-Time at end of window
1	1	1	27.82	26/01/1994 04:00
2	1	2	30.58	12/12/2011 22:00
3	1	5	34.48	15/01/1993 10:00
4	1	10	35.81	19/02/1997 18:00
5	1	20	37.65	08/12/1994 09:00
6	1	30	40.85	25/12/1990 10:00
7	3	1	58.59	17/01/2003 08:00
8	3	2	61.99	01/02/2014 22:00
9	3	5	71.2	08/12/1994 10:00
10	3	10	76.52	24/12/1989 17:00
11	3	20	78.38	03/12/1999 12:00
12	3	30	85.96	25/12/1990 11:00
13	6	1	79.68	19/12/1980 09:00
14	6	2	83.5	18/09/1989 02:00
15	6	5	88.46	03/01/2012 06:00
16	6	10	92.22	03/12/1999 14:00
17	6	20	93.49	24/12/1999 02:00
18	6	30	94.05	24/12/1989 19:00
19	12	1	92.02	05/05/1981 03:00
20	12	2	94.54	06/12/2001 03:00
21	12	5	96.11	30/10/1980 01:00
22	12	10	96.3	13/01/1984 17:00
23	12	20	97.45	15/01/1993 07:00
24	12	30	98.39	26/02/1990 08:00
25	24	1	96.28	21/01/2006 16:00
26	24	2	97.3	25/01/1986 19:00
27	24	5	97.94	26/10/1982 07:00

⁸ Event numbering is arbitrary. It is for the purpose of listing in the tables and referral in text.

28	24	10	98.42	26/02/1990 08:00
29	24	20	98.55	30/10/1980 02:00
30	24	30	98.85	22/08/2001 08:00

In order to observe and test the resilience of the energy system, it is important to understand what is occurring across Great Britain when a particular region experiences a ramping event. Figure 9 shows the most extreme event observed in a 6-hour time window in the 36-year time series for 'Offshore North', occurring on the 27th December 1998. Similar plots showing the most extreme event observed in a 6-hour time window in the 36-year time series for each region are provided in Appendix 9-12.

To put the event in Figure 9 into meteorological context, we can look at the synoptic chart for this day. In the early hours of the morning on 27th December 1998, there was a low pressure weather system sat to the north of Great Britain, resulting in very strong wind speeds over the 'Offshore North' region. This explains the extremely low capacity factor in Phase 1 of the 'Offshore North' plot (and in the early hours for 'Onshore North' also), where the wind speed was likely exceeding the turbine safety cut off, and therefore minimal (offshore) to low (onshore) generation was occurring in these northern regions. As the morning progresses and the weather system moved towards, the winds remained strong but decreased to below the safety cut-off. This is indicated in Phase 2 of the plot where the capacity factors across 'Offshore North' and 'Onshore North' are increasing again, causing the marked change in capacity factor over this time window.

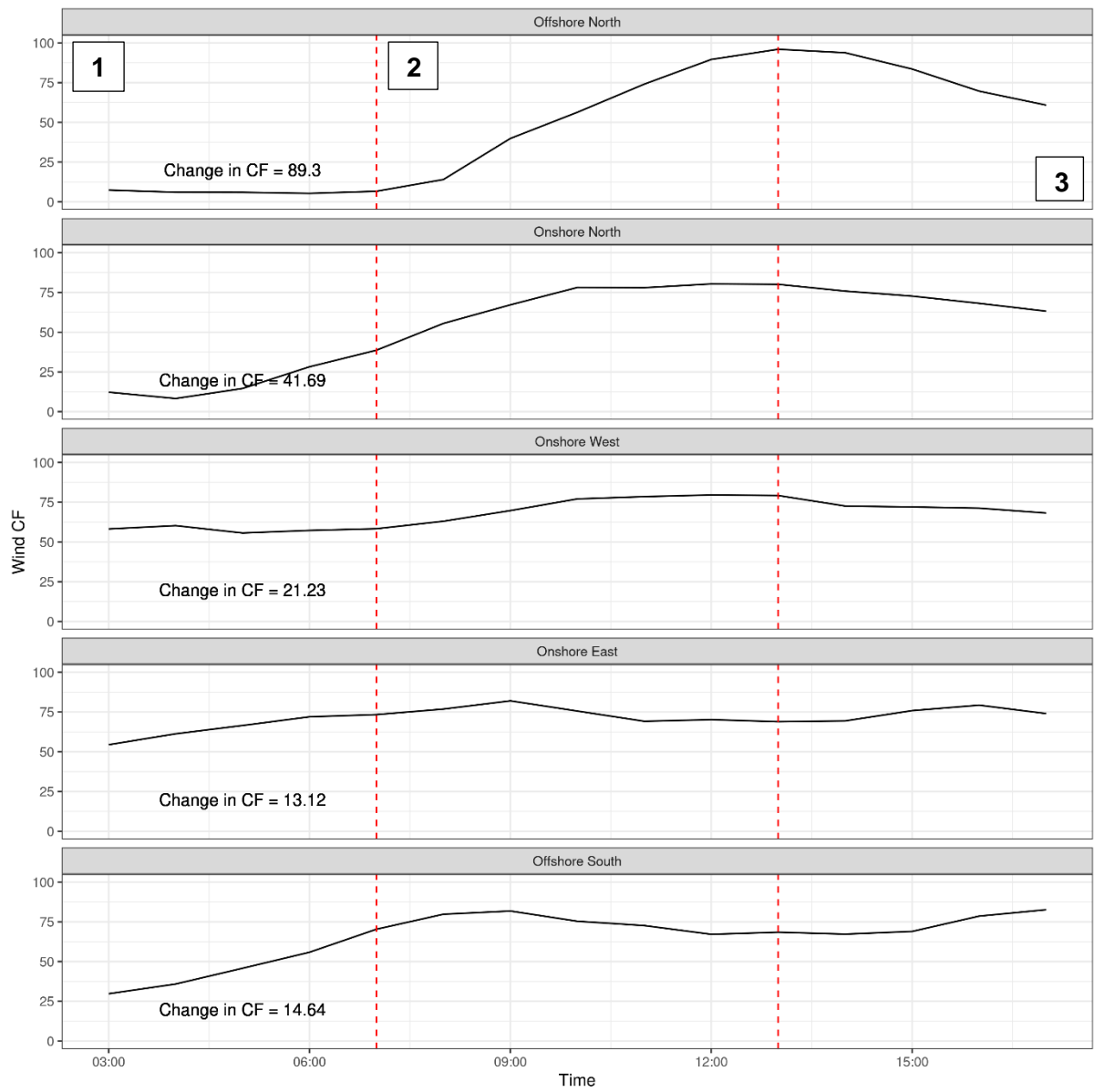


Figure 9: The most extreme event observed in a 6-hour time window in the 36-year timeseries for Offshore North (top row), occurred on the 27th December 1998. The capacity factor change over the same time window for the four other regions are presented to provide context of conditions elsewhere in Great Britain.

As the pressure system tracked over Scotland moving in a north-easterly direction, the southern regions experienced fairly consistent wind speeds and therefore a much smaller magnitude in capacity factor change over the same time period. Also, this track would likely have resulted in wind speeds over 'Onshore North' to have weakened earlier than over the 'Offshore North' region, shown by the increase in capacity factor from about 3am onshore as opposed to around 07:00 offshore, and the smaller magnitude in change observed in the 7am-1pm time window (ΔCF Offshore North = 89.3, ΔCF Onshore North = 41.69). Phase 3 of the plot, after the ramping event, is showing that wind speeds are likely to have decreased further as the low pressure system continued to move further east away from Great Britain.

Solar

In this section we build on the approach taken by Cannon et al. (2015) and apply this to solar renewables. We present the analysis of historical observed solar ramping events from the Euro4 data record, with equivalent plots to section 4.1.2 produced. This is done for each of the 3 solar regions separately.

4.2.1 Maximum change in capacity factor across defined regions over various time windows

Figure 10 shows, for a given time window on the x-axis, the number of times in an average year that the maximum change in capacity factor change (ΔCF) surpasses a particular change threshold (y-axis) for each of the defined regions for solar. The most extreme ramping event identified across the 36-year time series (1979-2014) are indicated by the dashed line. As an example, in an average year, the ΔCF surpassing at least 40 during a 12-hour time window in Scotland was observed between 100-1000 times, compared to 1000-4000 times in North England and South England and Wales (orange stars). For all regions, the most extremes change in capacity factor (the dashed line) increase rapidly with increasing time window up to ~6 hours, after which it starts to plateau. This corresponds to the length of time window after which weather driven ramping events are likely to be less significant than, or dampened by, the diurnal cycle of sunlight.

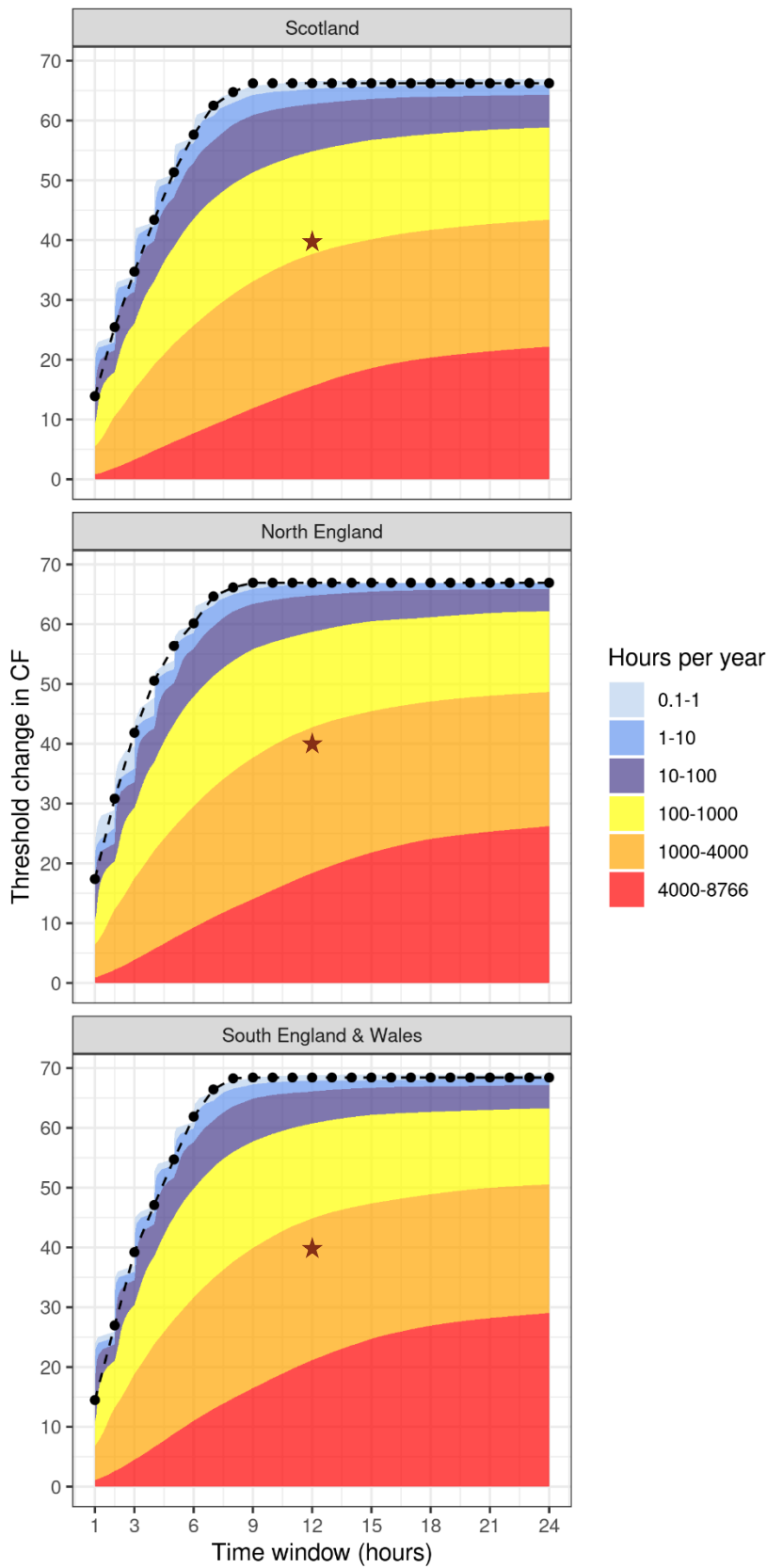


Figure 10: The frequency of hours for which there is a subsequent ramp in generation of at least ΔCF (y-axis) within the given time window (x-axis) for the defined regions of solar. The dashed lines mark the most extreme events in the 36-year time series (1979-2014).

When observing the number of times in an average year that a ramp event is observed reaching or exceeding a threshold of ΔCF for a given region and time window, as shown in Figure 11, it is possible to further examine the changes in events as the time window increases. Each line on the plot represents a different time window (1-, 3-, 6-, 12- and 24- hour time windows) with a row per a defined region – identified in the top grey bar. The right-hand panel presents an exploration of the less frequent ramping events for each region i.e., focusing on events reaching a threshold change less than 150 times (number of hours) in an average year. This shows that there are less frequent ramp events in the South England and Wales during the shorter time windows compared to Scotland and North England. For example, a ΔCF of 15 or more in a 1-hour time window was observed 75 times in an average year in South England and Wales, compared to 120 times in Scotland and 150 times in North England. This is also clearly shown in the 1- and 3- hour plots in the right-hand panel of Figure 12.

Figure 11 also highlights that the most frequent ramping events (occurring the most times in an average year) occur in the 12- and 24-hour time windows. Furthermore, in the right-hand panel of less frequent ramping events, the yellow and green lines representing the 12- and 24- hour time windows, respectively, are also tightly plotted i.e., events are occurring across a very similar, narrow range of threshold ΔCF . These results are to be expected given the strong diurnal cycle of solar, where the largest changes will be seen at sunrise and sunset.

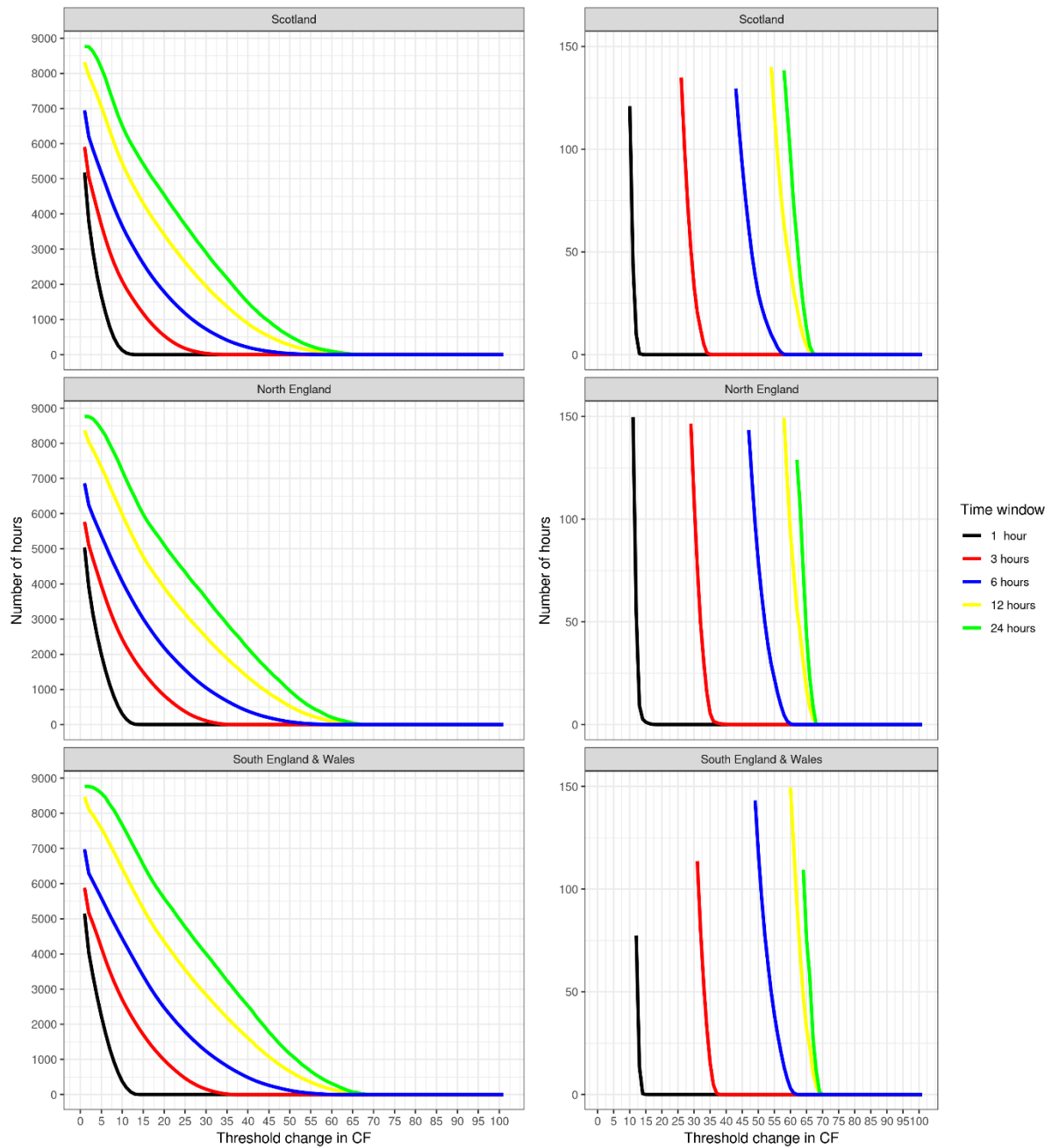


Figure 11: The number of hours in an average year (y-axis) that a ramp event is observed reaching or exceeding a threshold of ΔCF (x-axis). Each line on the plot represents a different time window (1-, 3-, 6-, 12- and 24- hour time windows) with a row per a defined region – identified in the top grey bar. The right-hand panel presents an exploration of the less frequent ramping events for each region i.e., focusing on events reaching a threshold change less than 150 times (number of hours) in an average year.

Similarly to Figure 11, Figure 12 presents the number of times in an average year (y-axis) that a ramp event reaches or exceeds a threshold of capacity factor change (x-axis), this time with a row for each time window with the events per region in an average year indicated by the coloured lines. This shows that Scotland experiences a smaller magnitude of change in capacity factor compared to North England and South West England and Wales, indicated by the orange line always falling to the left of the green and blue lines, with South West England

and Wales experiencing the highest magnitude of ΔCF . It is anticipated that this regional pattern should occur due to the climatological distribution of sunshine over Great Britain where, on average, the south experiences up to 30% more sunshine hours annually in comparison to Scotland⁹ i.e. the diurnal cycle weakens with latitude. As noted in section 3.2, it is the stronger correlation of incoming solar radiation with latitude rather than longitude which dictated the regional definitions, which is supported by these results.

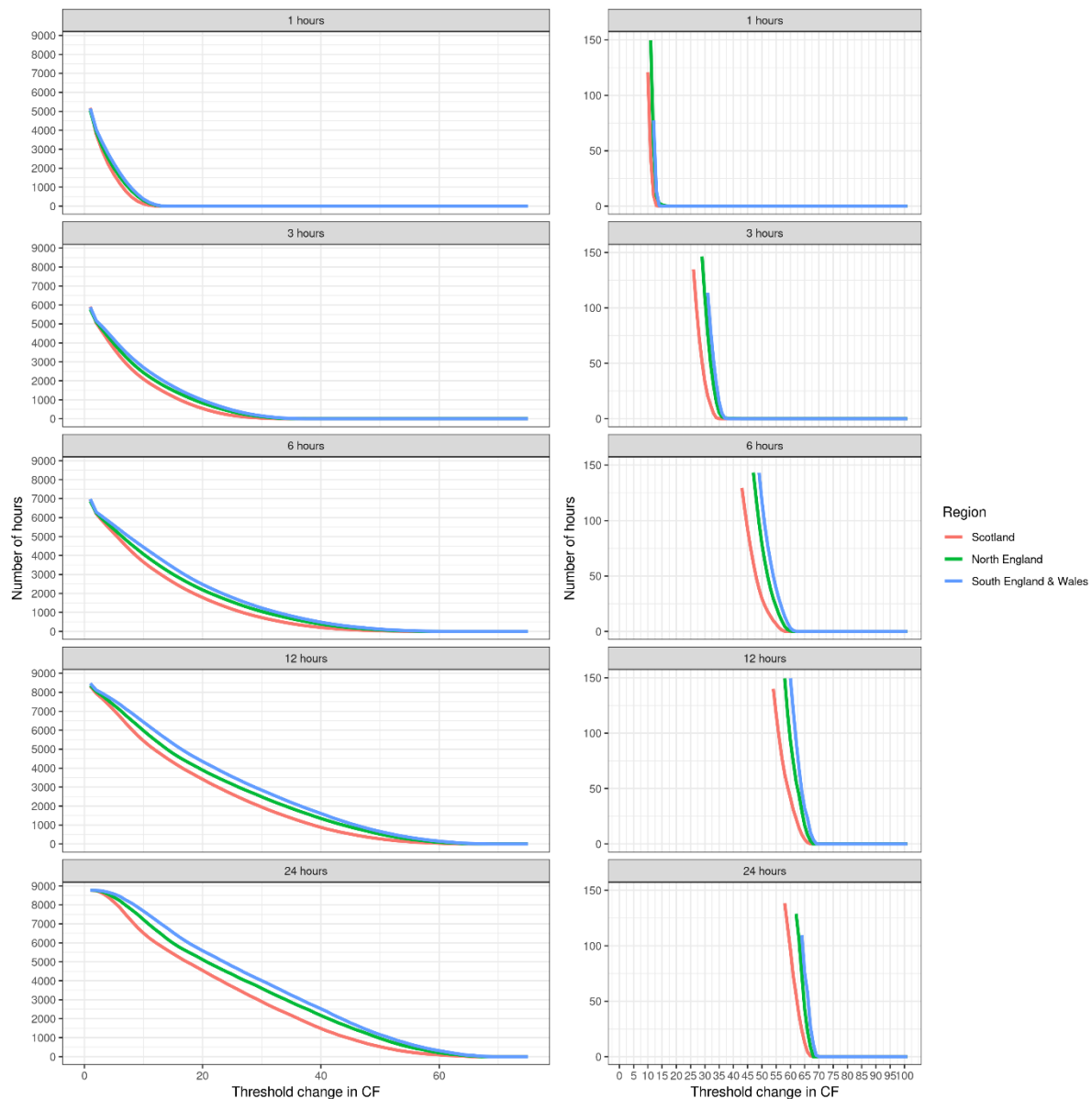


Figure 12: The number of hours in an average year (y-axis) that a ramp event is observed reaching or exceeding a threshold of ΔCF (x-axis). Each line on the plot represents a different defined region with a row per a time window – identified in the top grey bar. The right-hand panel presents an exploration of the less frequent ramping events for each time window i.e., focusing on events reaching a threshold change less than 150 times (number of hours) in an average year.

⁹ Observed from the Met Office UK average map for sunshine duration, annual average from 1981-2010 (<https://www.metoffice.gov.uk/research/climate/maps-and-data/uk-climate-averages/>)

As for wind, plots to explore the interannual and seasonal variability of solar ramping events in an average year were produced for the different regions, and are Appendix 13 and 14, respectively.

Appendix 13 shows minimal year-to-year variability in solar ramping events occurring in the 3, 6- and 12- hour time windows, particularly in the 3-hour time window and the least frequent events where the standard deviation around the mean, minimum and maximum events are almost indistinguishable.

In comparison to the wind ramping events, Appendix 14 indicates a much greater seasonal variation across regions in a 12-hour time window. The least frequent and small ΔCF changes appear to occur most often in winter and autumn with these seasonal lines falling below summer, spring and the average season. Conversely, the more frequent and greater ΔCF changes occur in summer and spring. It has already been noted that the largest changes in capacity factor causing solar ramping events over these longer time windows is the change from day-to-night or night-to-day. The similar seasonal pattern of summer and spring is likely the result of the longer periods of daylight hours in these months i.e., there is more time available during the window for an event to occur in comparison to shorter days. The length of daylight hours and the length of time for the sun to rise or set is impacted seasonally by the angle the Earth, or more specifically in this case the northern hemisphere, in relation to the sun. The longest day and shortest night of the year occurs on the summer solstice – when the northern hemisphere is fully tilted towards the Sun - and the shortest day and longest night occurs on the winter solstice – when the northern hemisphere is tilted fully away from the Sun¹⁰. The summer solstice is the astronomical definition of seasons and occurs in mid to late June – i.e., the longest day of the year occurs approximately half-way through the meteorological spring and summer seasons. This explains why spring and summer behave similarly, when intuitively you may expect summer (June-July-August) to have the longest days.

Given the lack of data on the seasonality of particular sky conditions and cloud coverage, it is not feasible to describe this seasonal pattern in the context of the frequency of clear-sky vs mixed-sky conditions.

¹⁰ <https://www.metoffice.gov.uk/weather/learn-about/met-office-for-schools/other-content/other-resources/our-seasons>

4.2.2 Return periods and return levels of extreme events

Figure 13 presents the results of the empirical extreme value analysis, carried out to calculate the return period ('expected' number of years in between events) of wind ramping events of a given return level (extremity of 'change in CF'). The left-hand panel presents the return period (x-axis) and return level (y-axis) for a time window (each coloured line) within a defined region (each plot). This supports the conclusions of section 4.2.1 that the most extreme events occur in the 12- and 24- hour time windows. Conversely, the right-hand panel presents the return period (x-axis) and return level (y-axis) for a defined region (each coloured line) within a given time window (each plot). This shows little variation between the defined regions and different return periods, other than supporting the observations from Figure 12 that Scotland experiences a smaller magnitude of change in capacity factor compared to North England and South West England and Wales.

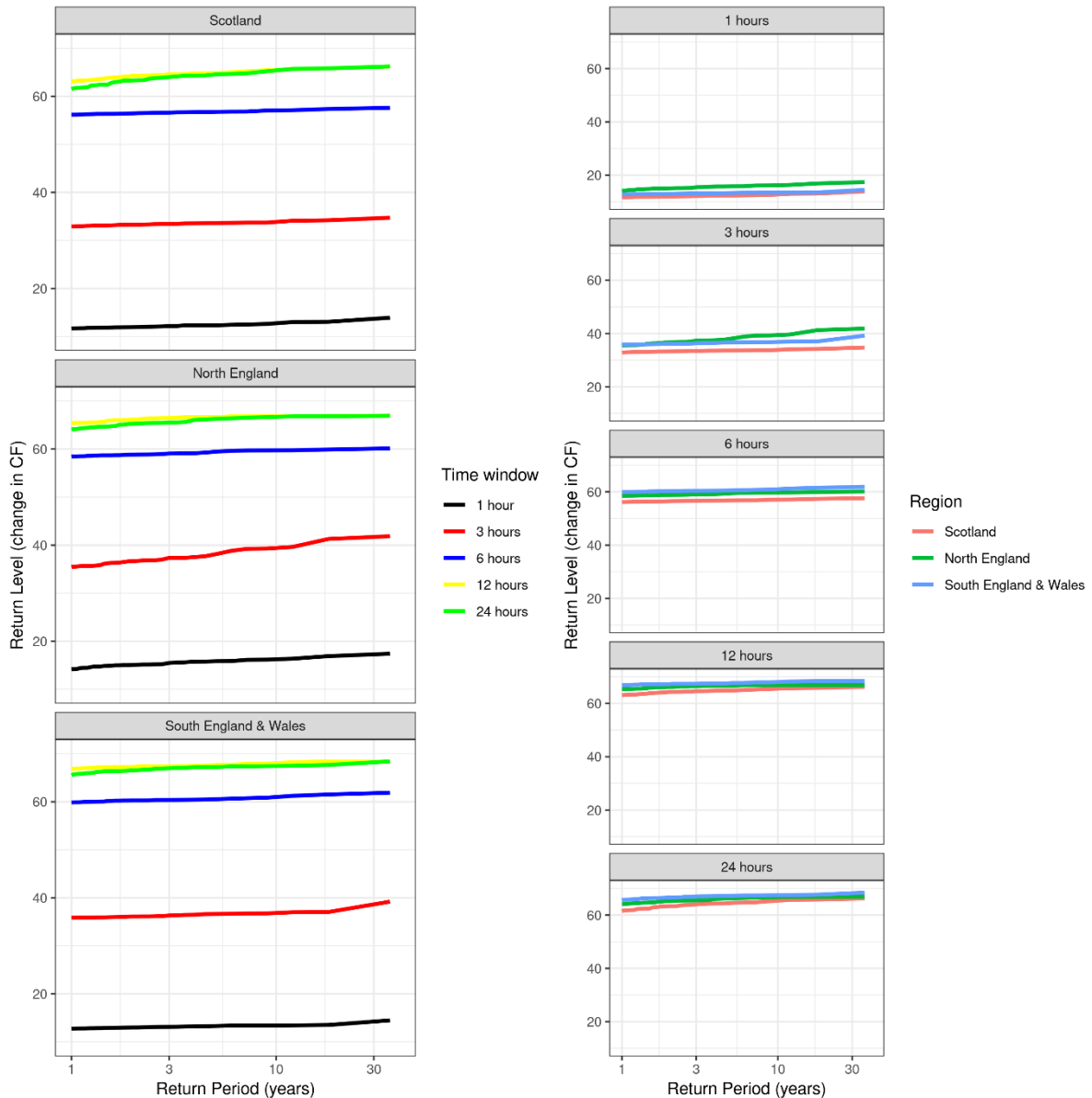


Figure 13: The return period (number of years in between events, x-axis) of wind ramping events of a given return level (extremity of 'change in CF', y-axis) for each time window and region combination. The left-hand panel presents each time window within a defined region. Conversely, the right-hand panel presents each defined region within a given time window.

A conclusion of this analysis has been that the use of large regions (and resulting averaging of grid cell capacity factors) has smoothed out the capacity factor changes resulting from cloud induced fluctuations in incoming solar radiation and therefore, particularly in time windows greater than 6-hours, the events captured by this analysis are mostly reflective of the diurnal cycle, as opposed to other, more unpredictable weather-driven ramping events. This explains why a 1 in 1 year event looks very similar to a 1 in 30-year event in the same time window – the same diurnal cycle is occurring in each year. For this reason, a selection of example events across the different time windows and return periods for the three regions have been included in Appendix 15-17 only, as opposed to the main report.

However, Figure 14 shows the most extreme capacity factor change event observed in a 1-hour time window within the 36-year timeseries in the North England region. Similar plots for the two other regions are included in Appendix 18 and 19.

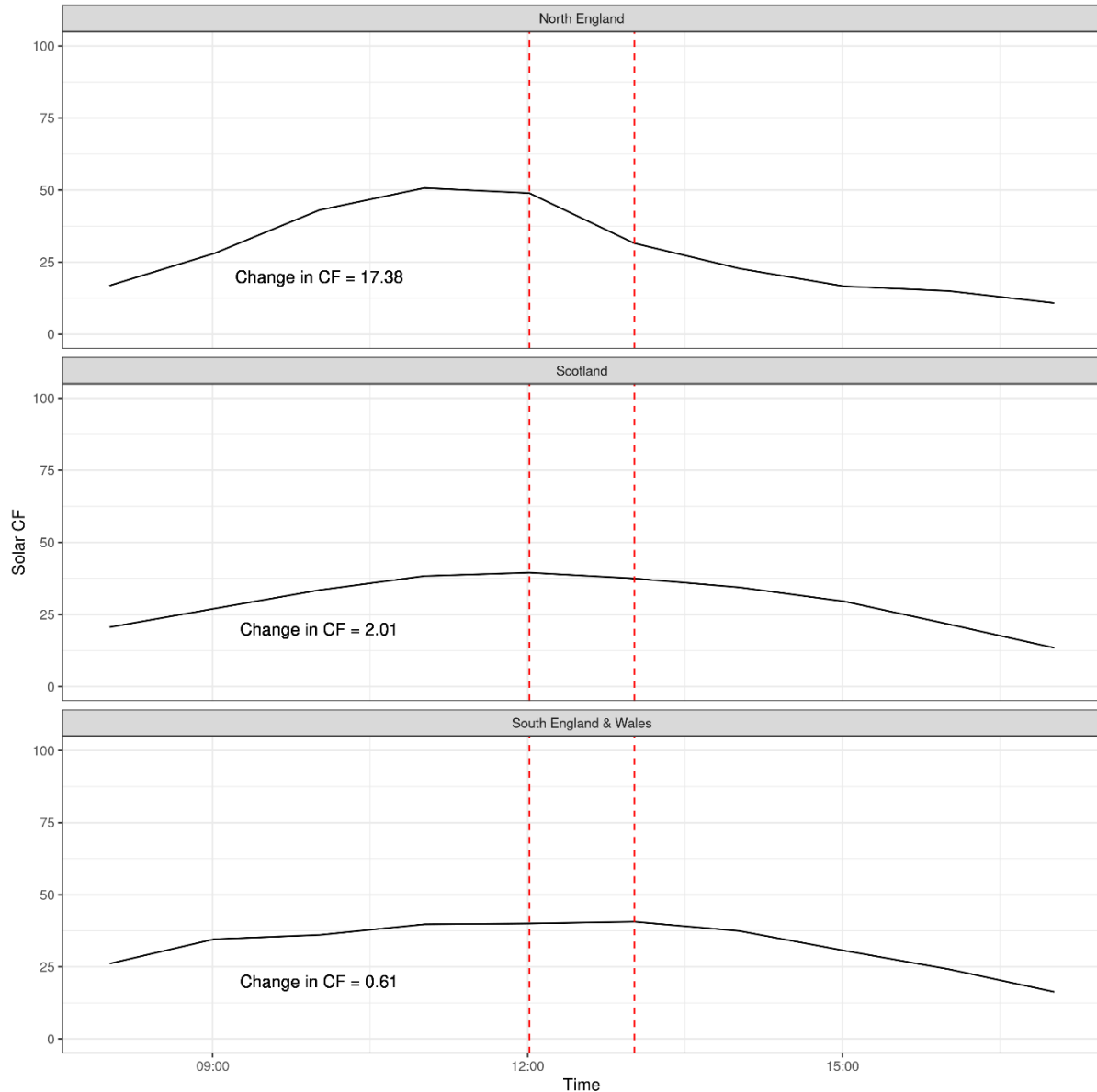


Figure 14: The most extreme event observed in a 1-hour time window in the 36-year timeseries for North England (top row). The capacity factor change over the same time window for Scotland (second row) and South England and Wales (bottom row) regions are presented to provide context of conditions in the other regions.

The event shown in Figure 14 occurs in the middle of the day on the 5th August 2003 and appears to be independent of conditions occurring in the other regions, and is therefore likely to be an example of a non-diurnal cycle related ramping event. This would suggest there is value in focusing future work in characterising short-duration solar ramping events on shorter time windows where weather driven ramping events are likely to be less dampened by, and occur at other day times to, the predictable capacity factor change associated with the diurnal

cycle. Another suggestion is the use of grid-cell data or aggregation into much smaller regions, to prevent smoothing of weather driven ramping events as seen in this analysis. A further suggestion from a research area expert would be to compare the predictable solar ramping events e.g., morning and evening, with occurrences in the historical period of simultaneous wind ramping events and the weather patterns associated with these joint occurrences that could stress the system.

5 Summary and Conclusion

This report has presented a method for characterising short-duration wind and solar ramping adverse weather events for renewable electricity system resilience testing, based on the meteorological conditions in a region. The approach has adopted the method of Cannon et al. (2015) (for calculating changes in capacity factor over various time windows) in combination with methods developed in the previous phase (for estimating wind and solar energy capacity factors from meteorological data) detailed in Dawkins and Rushby (2021) and Dawkins et al. (2021b). Similar to previous phases of this work, this approach aims to keep the characterisation of adverse weather as independent of a particular future electricity system as possible. This is achieved by using the ‘potential’ for installed wind or solar capacity in each grid cell (using insights from Price et al. (2018)), rather than a current day or future representation of where wind turbines or solar panels are actually located.

Great Britain has been separated into smaller regions for onshore wind, offshore wind and solar to reflect the climatological variation of meteorological variables. Within a region, a short-duration ramping event has been quantified as the maximum change in capacity factor, within a given time window – with the explored time windows adopted from Cannon et al. (2015) (1 hour, 3 hours, 6 hours, 12 hours and 24 hours). For a given time window e.g., 3 hours and region e.g., Scotland, the number of times a ‘maximum capacity factor change’ surpasses a particular change threshold was calculated, followed by the average number of ramping events per year that surpass each change threshold of interest. Finally, an Extreme Value Analysis was used to calculate the observed return period (number of years in between events) of ramping events of a given return level (extremity of ‘change in CF’). This identified 1 in 2, 5, 10, 20 and 30-year return period wind and solar ramping events for each region and time window combination observed in the Euro4 hindcast dataset. Examples of the short-duration wind and solar ramping events identified in the historical period for each wind and solar region have been presented, alongside a comparison to the results of Cannon et al. (2015) for Great Britain.

The results presented for wind ramping events are consistent with those produced by Cannon et al. (2015), although some small variation exists due to differing turbine allocation assumptions such as the difference in the wind power curves used and the different spatial distribution of wind turbines across Great Britain. Further differences include the wider domain used in this work, which was inclusive of a greater proportion of offshore wind turbine capacity, and the use of Euro4 hindcast data, which has a higher spatial resolution compared to MERRA

(4km instead of approximately 50km). A number of key observations resulting from the regional based analysis of wind ramping events are:

- In an average year, the number of times a ramp reaches a threshold of capacity factor change decreases as that threshold increases i.e., the higher thresholds are surpassed less often.
- A common feature across all the regions is that the maximum change in capacity factor (ΔCF) is larger during the bigger time windows, which is consistent with the findings of Cannon et al. (2015).
- In an average year, both offshore regions are observed to have smaller, less frequent ramps during the shorter time windows compared to the onshore regions.
- 'Onshore East' frequently experiences larger ΔCF during the shorter time windows.

Characterising solar ramping events has pushed the scope of the Cannon et al. (2015) approach, resulting in a number of regional and seasonal observations:

- In an average year, Scotland experiences a smaller magnitude of change in capacity factor compared to North England and South West England and Wales – this is likely due to the weakening of the diurnal cycle with latitude.
- In an average year, there are less frequent ramp events in South England and Wales during the shorter time windows compared to Scotland and North England.
- The more frequent and greater changes in capacity factor occur in summer and spring, likely as a result of the longer periods of daylight hours in these months.

However, improvements for future work have been identified to better capture the 'unpredicted' weather driven ramping events occurring on a smaller scale than the regions used for this analysis. These include a focus on the shorter time windows (where weather driven ramping events are more likely to be captured, as opposed to predictable capacity factor change associated with the diurnal cycle in longer time windows) and the use of grid-cell data or aggregation into much smaller regions, to prevent smoothing of small-scale cloud activity as seen in this analysis. As a follow up to this work, it may be interesting to compare the predictable solar ramping events e.g., sunrise and sunset, with occurrences in the historical period of simultaneous wind ramping events and the weather patterns associated with these joint occurrences that could stress the system.

This report has provided a validated method for characterising short-duration wind and solar ramping events for a highly renewable electricity system. Developing this method for characterising short-duration solar ramping events has shown that analysis is required to focus on shorter time windows over smaller regions in order to fully capture the meteorological

conditions that result in a ramping event outside of the diurnal cycle (i.e. due to the movement of clouds across a solar farm). Later phases of this project aim to apply the approach presented in this report to identify events within other meteorological datasets. It is known that the intended datasets do not contain solar data at a sufficient temporal resolution to overcome the learnings of this method development, and therefore the final adverse weather datasets for short-duration events will focus on wind ramping events only.

6 References

- Bett, P. E. and Thornton, H. C. (2016). The climatological relationships between wind and solar energy supply in Britain. *Renewable Energy*, 87:96–110.
- Bloomfield, H. C. et al., 2018. The changing sensitivity of power systems to meteorological drivers: a case study of Great Britain. *Environmental Research Letters*, pp. 13, 054028.
- Burton, T., Sharpe, D., Jenkins, N., and Bossanyi, E. (2011). *Wind Energy Handbook*, Second Edition. Wiley, Chichester, West Sussex, UK.
- Butcher, T. and Dawkins, L. (2020). Adverse weather scenarios for renewable energy system testing: Discovery phase. Technical report.
- D. J. Cannon, D. J. Brayshaw, J. Methven, P. J. Coker and D. Lenaghan, Using reanalysis data to quantify extreme wind power generation statistics: A 33 year case study in Great Britain, *Renewable Energy*, 75:767-778, 2015.
- Coles, S. (2001). *An Introduction to Statistical Modelling of Extreme Values*. Springer
- Dawkins, L. and Rushby, I. (2021). Characterising adverse weather for the UK electricity system, including addendum for surplus generation events. Technical report.
- Dawkins, L., Rushby, I., Pearce, M., Wallace, E. and Butcher, T. (2021a): Adverse Weather Scenarios for Future Electricity Systems. NERC EDS Centre for Environmental Data Analysis. Available at:
<https://catalogue.ceda.ac.uk/uuid/7beeed0bc7fa41feb10be22ee9d10f00>
- Dawkins, L., Rushby, I. and Pearce, M. (2021b). Adverse Weather Scenarios for Future Electricity Systems: Developing the dataset of long-duration events. Technical report.
- Drew, D. R., Cannon, D. J., Barlow, J. F., Coker, P. J., and Frame, T. H. A. (2017). The importance of forecasting regional wind power ramping: A case study for the UK. *Renewable Energy*, 114, Part B:1201–2018.
- IEC (2005). International standard IEC 61400-1 (third edition). Technical report.
- Lohmann, G. M., Monahan, A. H., and Heinemann, D. (2016). Local short-term variability in solar irradiance. *Atmospheric Chemistry and Physics*, 16:6365–6379.
- Moore, A., Price, J., and Zeyringer, M. (2018). The role of floating offshore wind in a renewable focused electricity system for great britain in 2050. *Energy Strategy Reviews*, 22:270–278.
- nationalgridESO (2019). De-rating factor methodology for renewables participation in the capacity market, consultation response summary. Technical report.
- Price, J., Mainzer, K., Petrović, S., Zeyringer, M., and McKenna, R. (2020). The implications of landscape visual impact on future highly renewable power systems: a case study for great britain. *IEEE Transactions on Power Systems*, pages 1–1.
- Price, J., Zeyringer, M., Konadu, D., Mourao, Z. S., Moore, A., and Sharp, E. (2018). Low carbon electricity systems for great britain in 2050: An energy-land-water perspective. *Applied Energy*, 228:928941.

Sinden, G. (2007). Characteristics of the UK wind resource: Long-term patterns and relationship to electricity demand. *Energy Policy*, 35(1):112–127

Watson, S. (2014). Quantifying the variability of wind energy. *Wiley Interdisciplinary Reviews - Energy and Environment*, 3(4):330–342.

7 Glossary

CEDA = Centre for Environmental Data Analysis

CDD = Cooling Degree Days

CF = Capacity Factor

Δ CF = Change in Capacity Factor

EVA = Extreme Value Analysis

GB = Great Britain

HDD = Heating Degree Days

IEC = International Electrotechnical Commission

MERRA = Modern-Era Retrospective analysis for Research and Applications

NEWA = New European Wind Atlas

SGI = Surplus Generation Index

UKCP18 = United Kingdom Climate Projections 2018

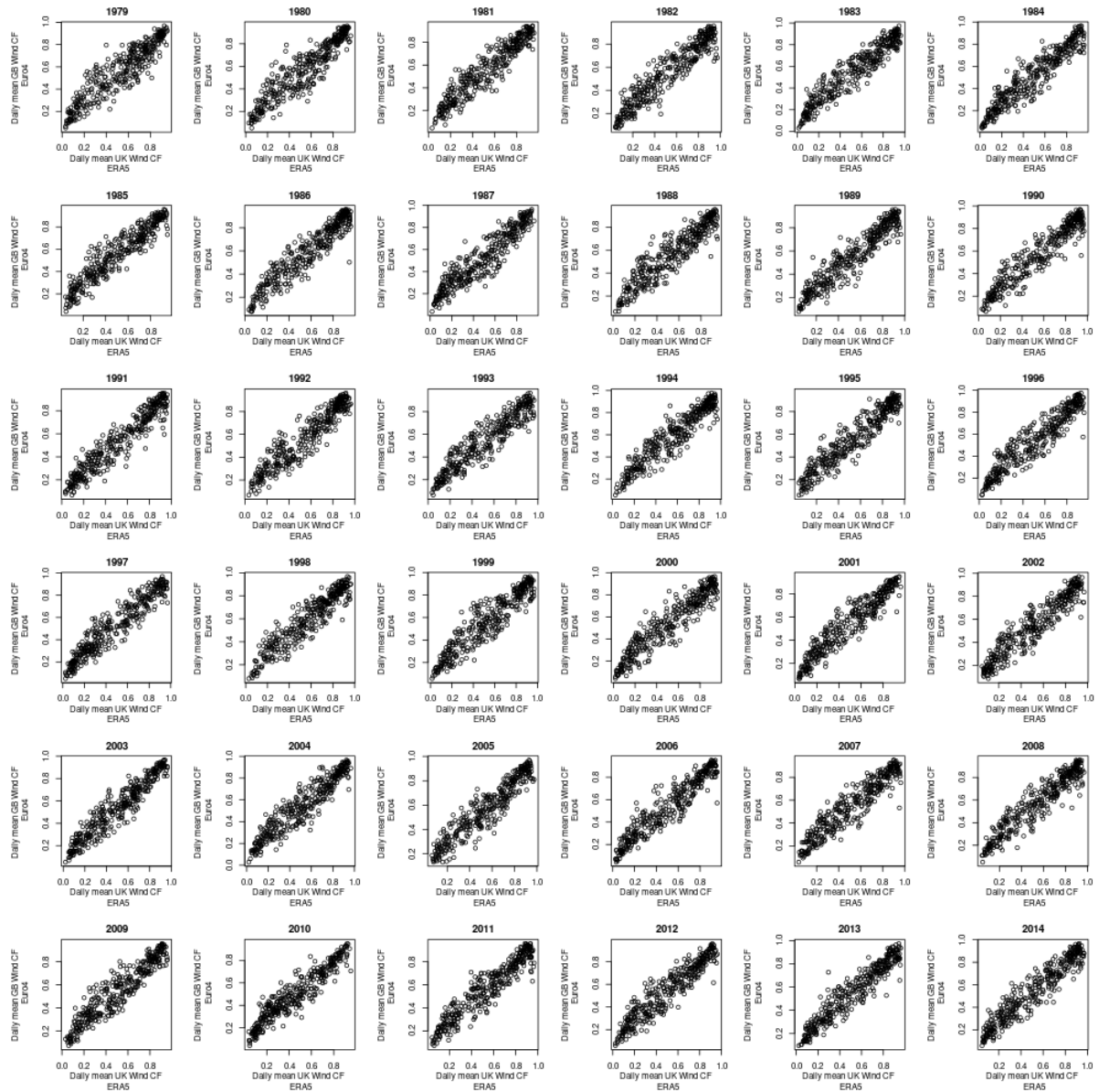
WDD = Weather Dependent Demand

WDI = Wind Drought Index

8 Appendix

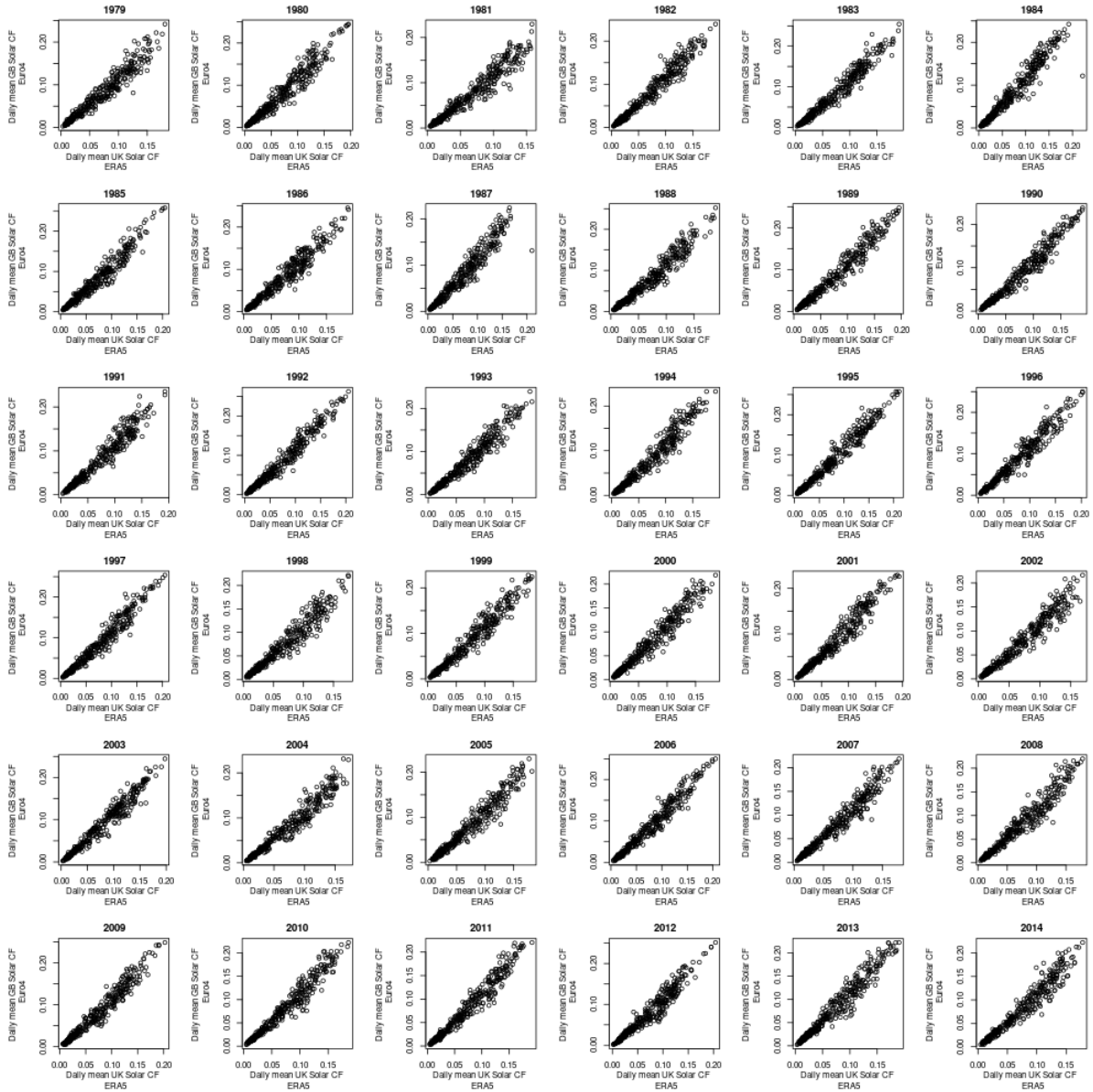
Appendix 1

Validation of daily wind capacity factors calculated using Euro4 hindcast data against those calculated in phase 2 using ERA5 reanalysis data.



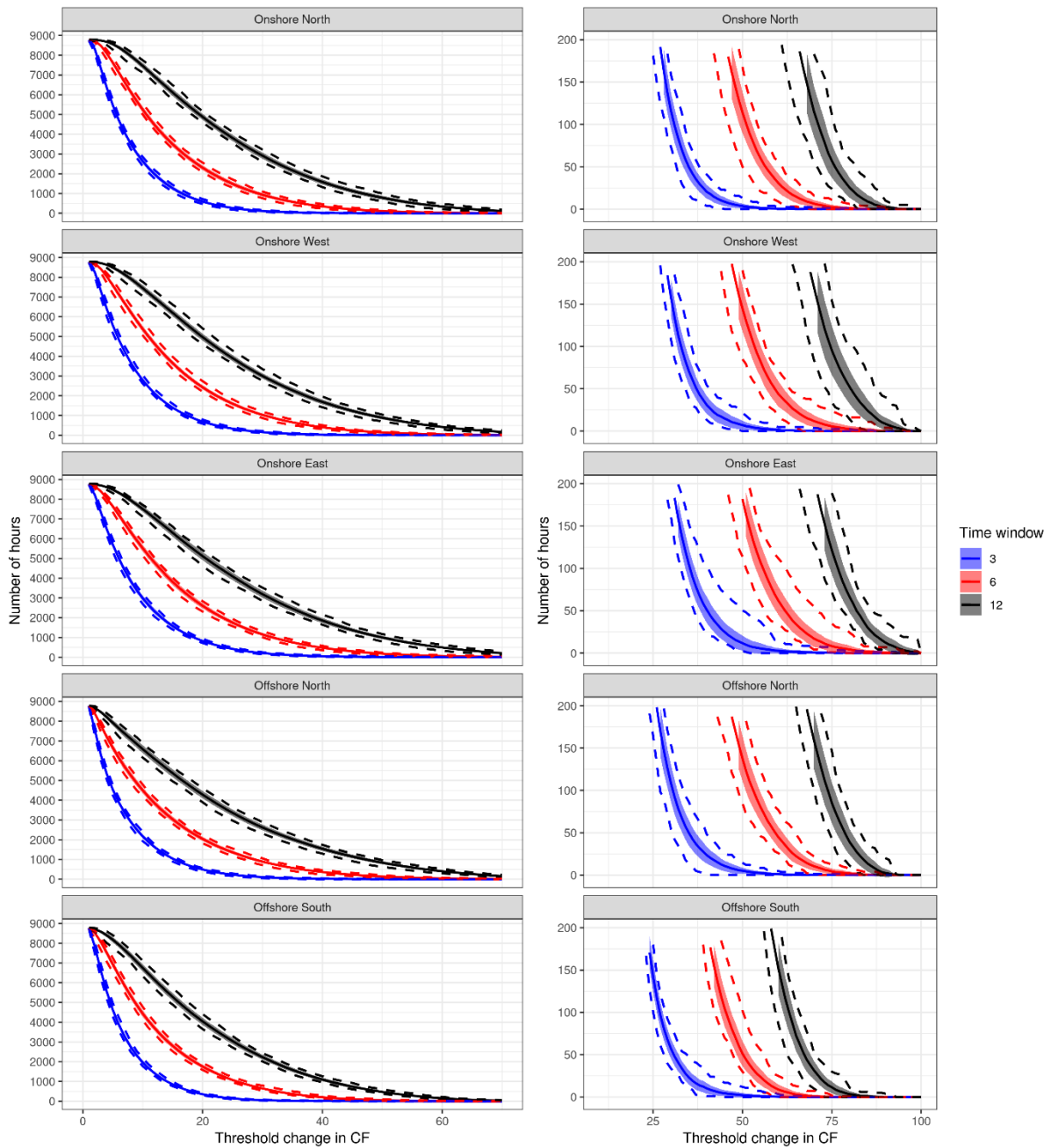
Appendix 2

Validation of daily solar capacity factors calculated using Euro4 hindcast data against those calculated in phase 2 using ERA5 reanalysis data.



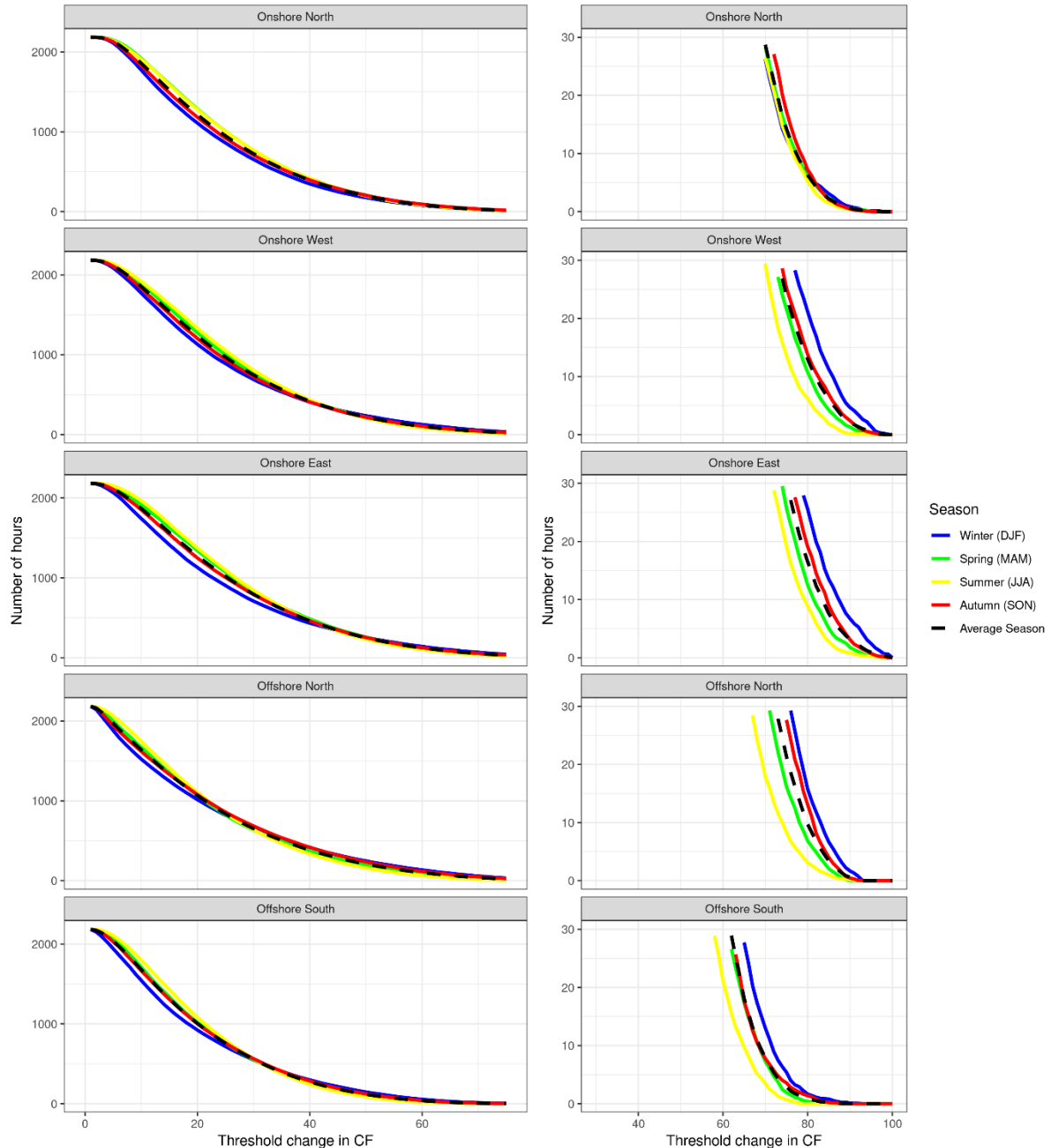
Appendix 3

The number of times (y-axis) that a wind ramp event reaches or exceeds a threshold of capacity factor change (x-axis) for three different time windows (3-, 6- and 12-hours), shown for each defined wind region. For each time window, the shaded area shows the frequency in a mean year ± 1 standard deviation and the dashed lines show the highest and lowest number that occurred in any one year. The right-hand panel presents an exploration of the less frequent ramping events for each time window or season i.e., focusing on events reaching a threshold change less than 200 times (number of hours) in an average year. In the right-hand panel plots, the shaded region deviates to the right of the mean line. This is the result of the plotting functionality in R when truncating a shaded region and therefore this plot should only be interpreted for y in (0,100) when observing the standard deviation around the mean.



Appendix 4

The number of times that a wind ramp event reaches or exceeds a threshold of capacity factor change (x-axis) for an average season and the four meteorological seasons (winter, spring, summer and autumn) in a 12-hour time window for each defined wind region. The right-hand panel presents an exploration of the less frequent ramping events for each time window or season i.e., focusing on events reaching a threshold change less than 30 times (number of hours) in an average year.



Appendix 5

Example wind ramping events observed in the Euro4 hindcast dataset in 'Offshore North' for different time windows and return periods. The first column indicates the length of the time-window in which an event was observed. The second column indicates the return period i.e., number of years in between events. The third column indicates the observed return level (extremity of 'change in CF'). The fourth column indicates the date/time for the end of the window in which the event occurred.

	Time window (hours)	Return period (years)	Return level (change in CF)	Date-Time at end of window
1	1	1	23.89	16/12/1979 18:00
2	1	2	28.07	29/10/1984 09:00
3	1	5	31.38	01/02/1983 02:00
4	1	10	32.19	22/12/1999 19:00
5	1	20	32.92	03/04/1998 04:00
6	1	30	33.24	17/01/1995 20:00
7	3	1	56.7	03/02/2011 19:00
8	3	2	60.91	14/10/1998 10:00
9	3	5	65.18	20/11/1981 22:00
10	3	10	68.41	01/02/1983 04:00
11	3	20	74.8	06/11/1996 09:00
12	3	30	77.32	11/01/1984 16:00
13	6	1	77.62	12/12/2003 04:00
14	6	2	81.61	29/10/1984 12:00
15	6	5	86.41	20/12/1989 04:00
16	6	10	87.3	02/11/2003 04:00
17	6	20	88.46	11/01/1984 18:00
18	6	30	89.3	27/12/1998 13:00
19	12	1	87.7	23/02/1992 16:00
20	12	2	89.97	04/01/2012 01:00
21	12	5	91.39	27/12/1998 00:00
22	12	10	91.78	12/12/2003 16:00
23	12	20	92.05	10/11/2002 11:00
24	12	30	92.44	17/01/2007 06:00
25	24	1	92.02	16/09/1992 16:00
26	24	2	92.61	11/02/2011 22:00
27	24	5	94.49	23/03/2000 23:00
28	24	10	95.05	14/03/2014 20:00
29	24	20	95.77	12/05/1992 01:00
30	24	30	96.37	14/04/2013 00:00

Appendix 6

Example wind ramping events observed in the Euro4 hindcast dataset in 'Offshore South' for different time windows and return periods. The first column indicates the length of the time-window in which an event was observed. The second column indicates the return period i.e., number of years in between events. The third column indicates the observed return level (extremity of 'change in CF'). The fourth column indicates the date/time for the end of the window in which the event occurred.

	Time window (hours)	Return period (years)	Return level (change in CF)	Date-Time at end of window
1	1	1	26.52	02/01/1984 19:00
2	1	2	30.32	10/03/2008 12:00
3	1	5	34.47	16/01/1984 20:00
4	1	10	38.77	21/01/1995 15:00
5	1	20	41.76	13/01/1984 02:00
6	1	30	41.87	13/12/2000 02:00
7	3	1	49.8	18/01/2007 22:00
8	3	2	55.04	25/12/1990 16:00
9	3	5	59.31	03/12/1999 14:00
10	3	10	63.77	03/01/2012 07:00
11	3	20	64.77	03/12/1999 08:00
12	3	30	67.01	10/03/2008 09:00
13	6	1	65.56	21/01/1995 22:00
14	6	2	68.67	05/06/2003 00:00
15	6	5	74.27	26/02/1990 09:00
16	6	10	75.95	16/12/2004 01:00
17	6	20	78.91	13/01/1984 02:00
18	6	30	79.97	03/01/2012 07:00
19	12	1	78.95	27/12/2004 20:00
20	12	2	81.32	07/10/1981 00:00
21	12	5	85.54	31/12/1999 03:00
22	12	10	86.53	17/11/1979 15:00
23	12	20	88.19	03/01/2012 07:00
24	12	30	91.71	18/01/1986 02:00
25	24	1	89.44	25/09/1991 11:00
26	24	2	90.74	03/08/1998 12:00
27	24	5	93.08	13/09/1993 02:00
28	24	10	93.31	17/11/1979 23:00
29	24	20	93.99	29/06/1989 20:00
30	24	30	94.24	29/03/1999 00:00

Appendix 7

Example wind ramping events observed in the Euro4 hindcast dataset in 'Onshore North' for different time windows and return periods. The first column indicates the length of the time-window in which an event was observed. The second column indicates the return period i.e., number of years in between events. The third column indicates the observed return level (extremity of 'change in CF'). The fourth column indicates the date/time for the end of the window in which the event occurred.

	Time window (hours)	Return period (years)	Return level (change in CF)	Date-Time at end of window
1	1	1	24.45	27/12/1979 13:00
2	1	2	26.81	31/12/2003 22:00
3	1	5	29.6	28/01/2002 19:00
4	1	10	32.23	23/12/2004 08:00
5	1	20	32.98	23/01/1990 03:00
6	1	30	35.08	03/02/2011 15:00
7	3	1	52.7	18/12/1992 04:00
8	3	2	56.74	24/12/1989 16:00
9	3	5	63.35	23/02/1997 09:00
10	3	10	66.47	10/02/2000 06:00
11	3	20	71.29	28/01/2002 19:00
12	3	30	79.78	03/02/2011 16:00
13	6	1	74.54	23/12/2004 12:00
14	6	2	79.16	10/06/1986 04:00
15	6	5	84.28	08/01/2005 01:00
16	6	10	85.17	28/01/2002 20:00
17	6	20	85.5	26/12/1998 18:00
18	6	30	91.08	03/02/2011 16:00
19	12	1	87.29	05/03/1981 21:00
20	12	2	90.59	28/05/1996 12:00
21	12	5	92.8	19/07/1998 04:00
22	12	10	93.74	13/03/1994 21:00
23	12	20	95.5	16/06/1983 00:00
24	12	30	96.32	14/02/1989 06:00
25	24	1	93.16	14/03/2002 20:00
26	24	2	94.37	20/08/1979 20:00
27	24	5	96.1	04/12/1979 17:00
28	24	10	96.91	05/09/2002 13:00
29	24	20	97.21	12/10/2009 12:00
30	24	30	97.74	12/01/2005 00:00

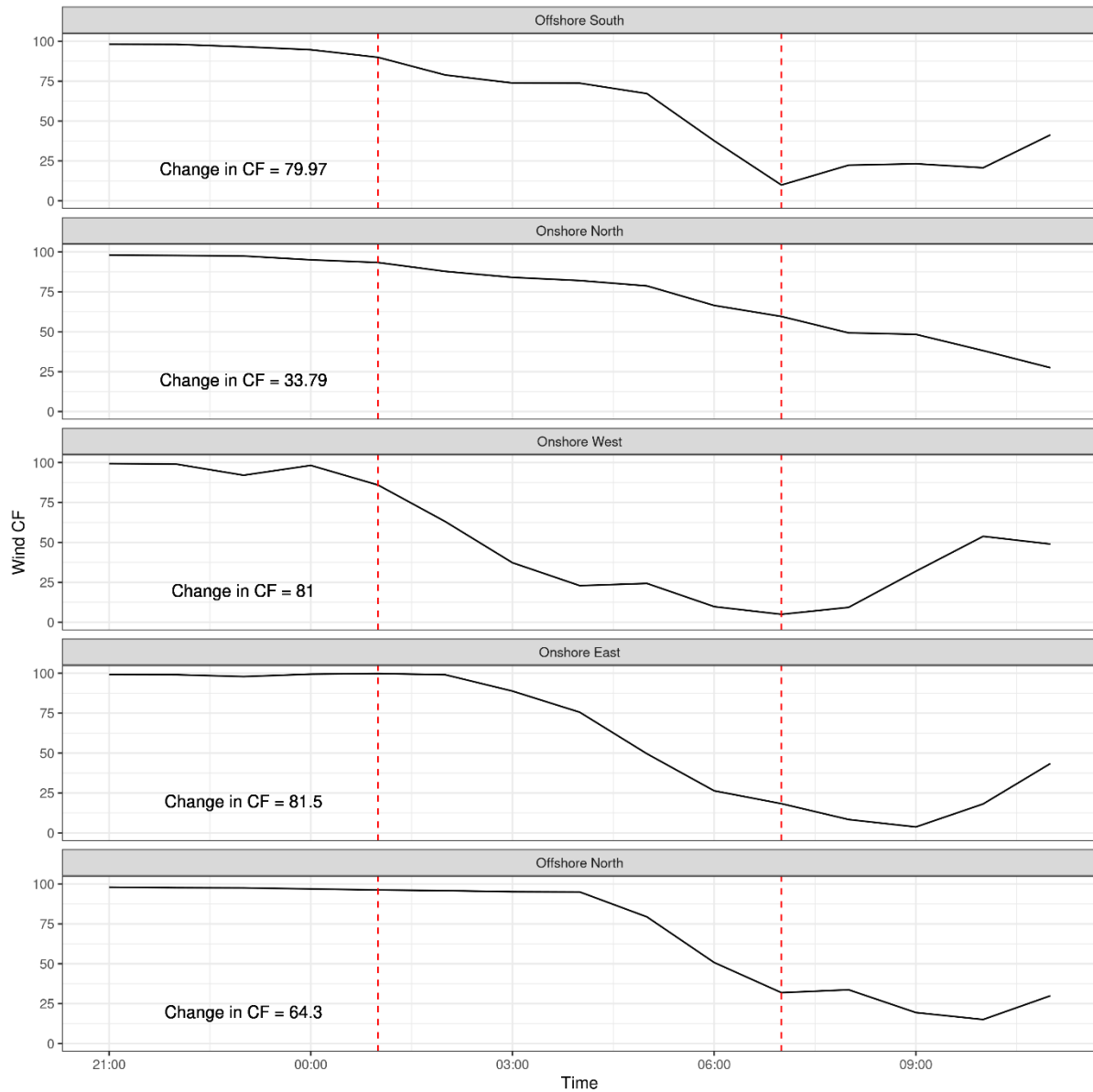
Appendix 8

Example wind ramping events observed in the Euro4 hindcast dataset in 'Onshore East' for different time windows and return periods. The first column indicates the length of the time-window in which an event was observed. The second column indicates the return period i.e., number of years in between events. The third column indicates the observed return level (extremity of 'change in CF'). The fourth column indicates the date/time for the end of the window in which the event occurred.

	Time window (hours)	Return period (years)	Return level (change in CF)	Date-Time at end of window
1	1	1	31.67	06/04/1991 09:00
2	1	2	34.65	15/10/1983 11:00
3	1	5	38.85	23/12/2013 13:00
4	1	10	43.41	03/12/1999 12:00
5	1	20	48.04	12/11/1991 20:00
6	1	30	48.97	13/01/1984 12:00
7	3	1	61.95	22/03/1981 19:00
8	3	2	67.54	08/12/1994 11:00
9	3	5	76.98	26/12/1998 17:00
10	3	10	82.28	23/12/2013 13:00
11	3	20	84.71	25/12/1990 13:00
12	3	30	92.81	03/12/1999 13:00
13	6	1	82.04	01/02/1990 20:00
14	6	2	85.77	15/01/1986 02:00
15	6	5	90.69	03/01/2012 08:00
16	6	10	93.04	13/01/1984 15:00
17	6	20	96.48	03/12/1999 14:00
18	6	30	98.43	25/12/1990 14:00
19	12	1	93.52	23/06/1994 06:00
20	12	2	95.21	06/10/2014 23:00
21	12	5	96.48	03/12/1999 14:00
22	12	10	98.16	26/02/1990 10:00
23	12	20	98.67	25/12/1990 18:00
24	12	30	98.73	12/03/1982 12:00
25	24	1	97.55	08/11/1989 23:00
26	24	2	98.29	23/09/2012 16:00
27	24	5	98.94	21/01/2001 11:00
28	24	10	99.22	17/07/2001 10:00
29	24	20	99.38	07/04/1993 09:00
30	24	30	99.64	30/10/1980 10:00

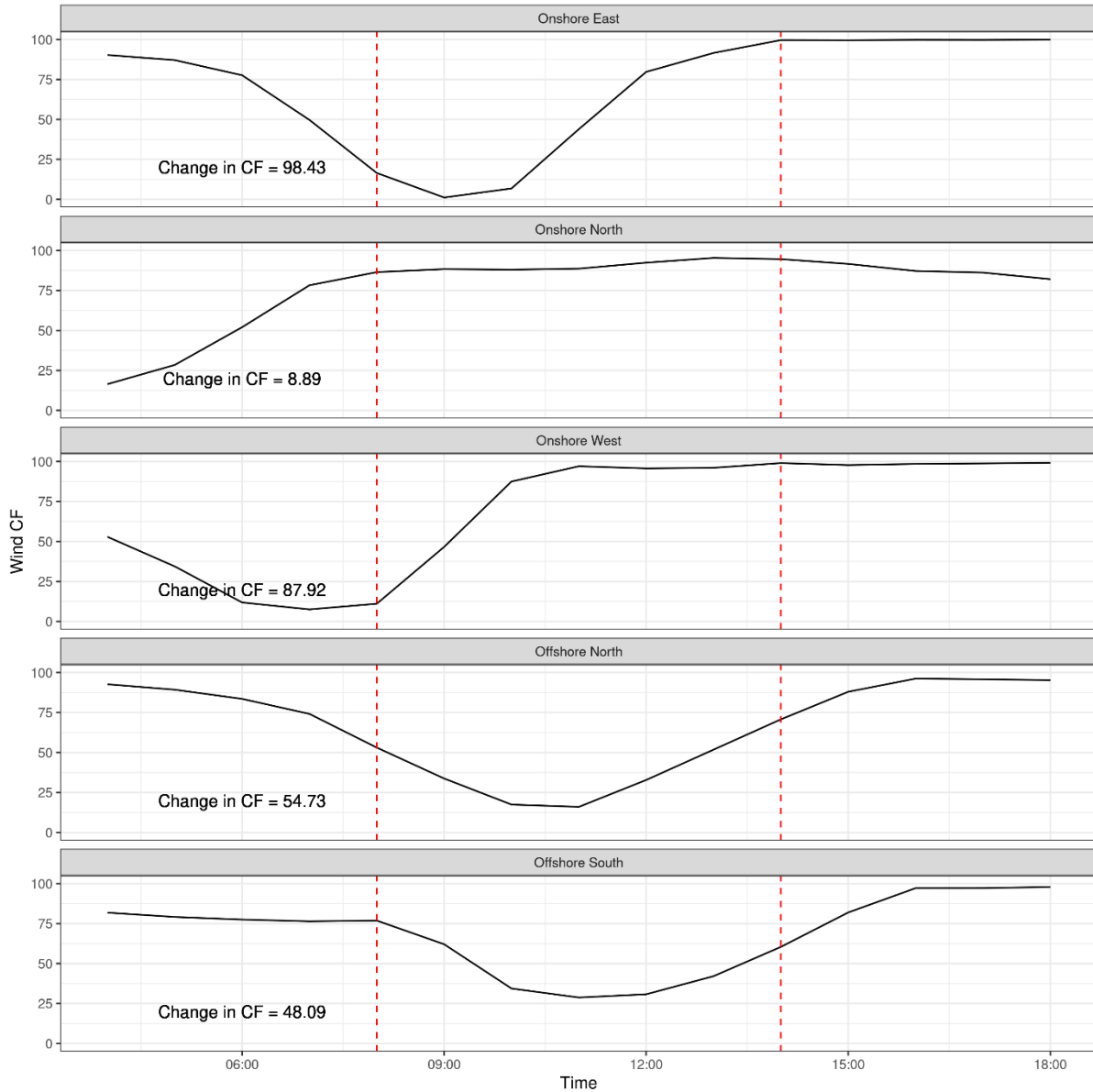
Appendix 9

The most extreme wind ramp event observed in a 6-hour time window in the 36-year timeseries for Offshore South (top row), occurred on the 3rd January 2012. The capacity factor change over the same time window for the four other regions are presented to provide context of conditions elsewhere in Great Britain.



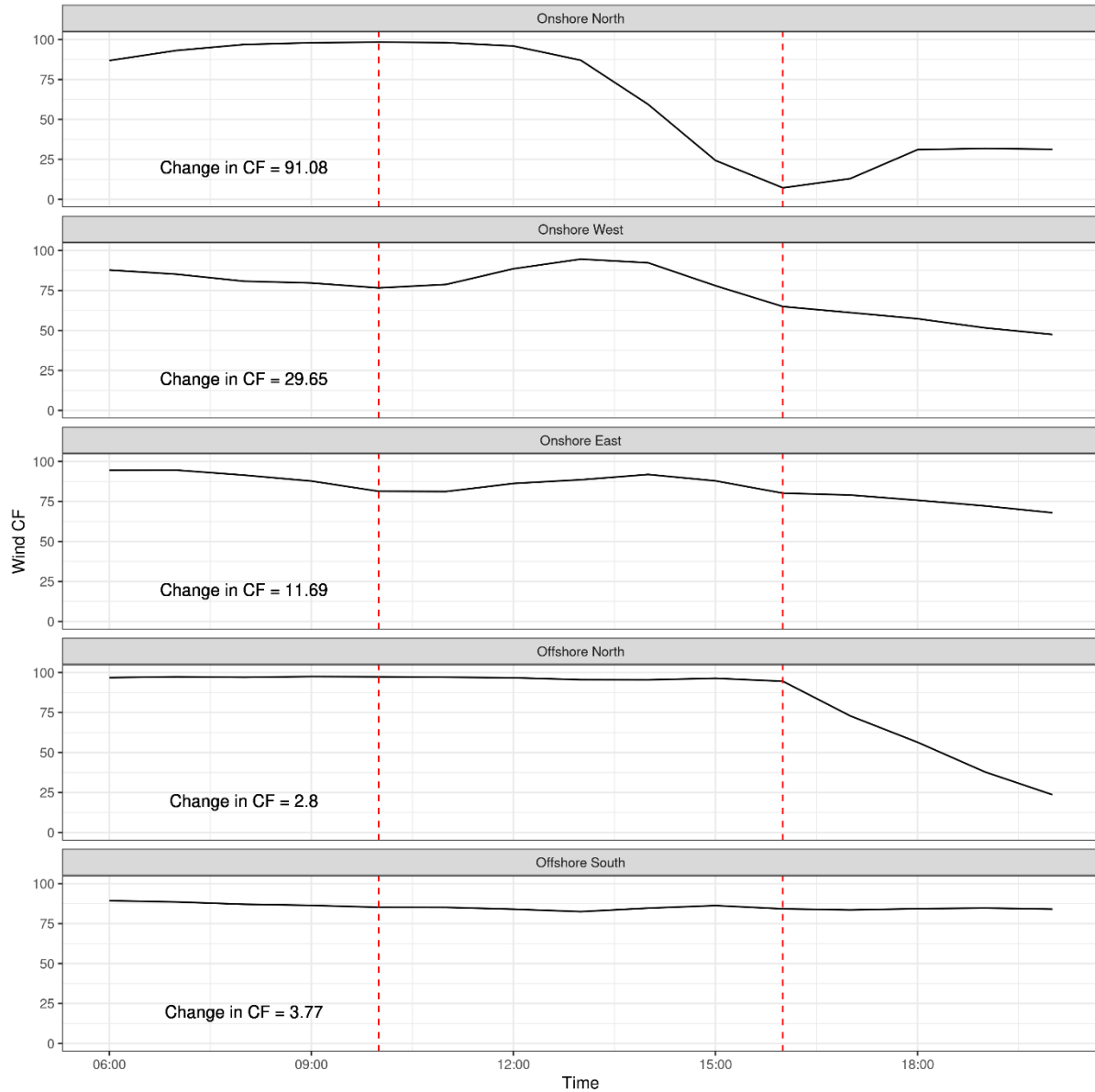
Appendix 10

The most extreme wind ramp event observed in a 6-hour time window in the 36-year timeseries for Onshore East (top row), occurred on the 25th December 1990. The capacity factor change over the same time window for the four other regions are presented to provide context of conditions elsewhere in Great Britain.



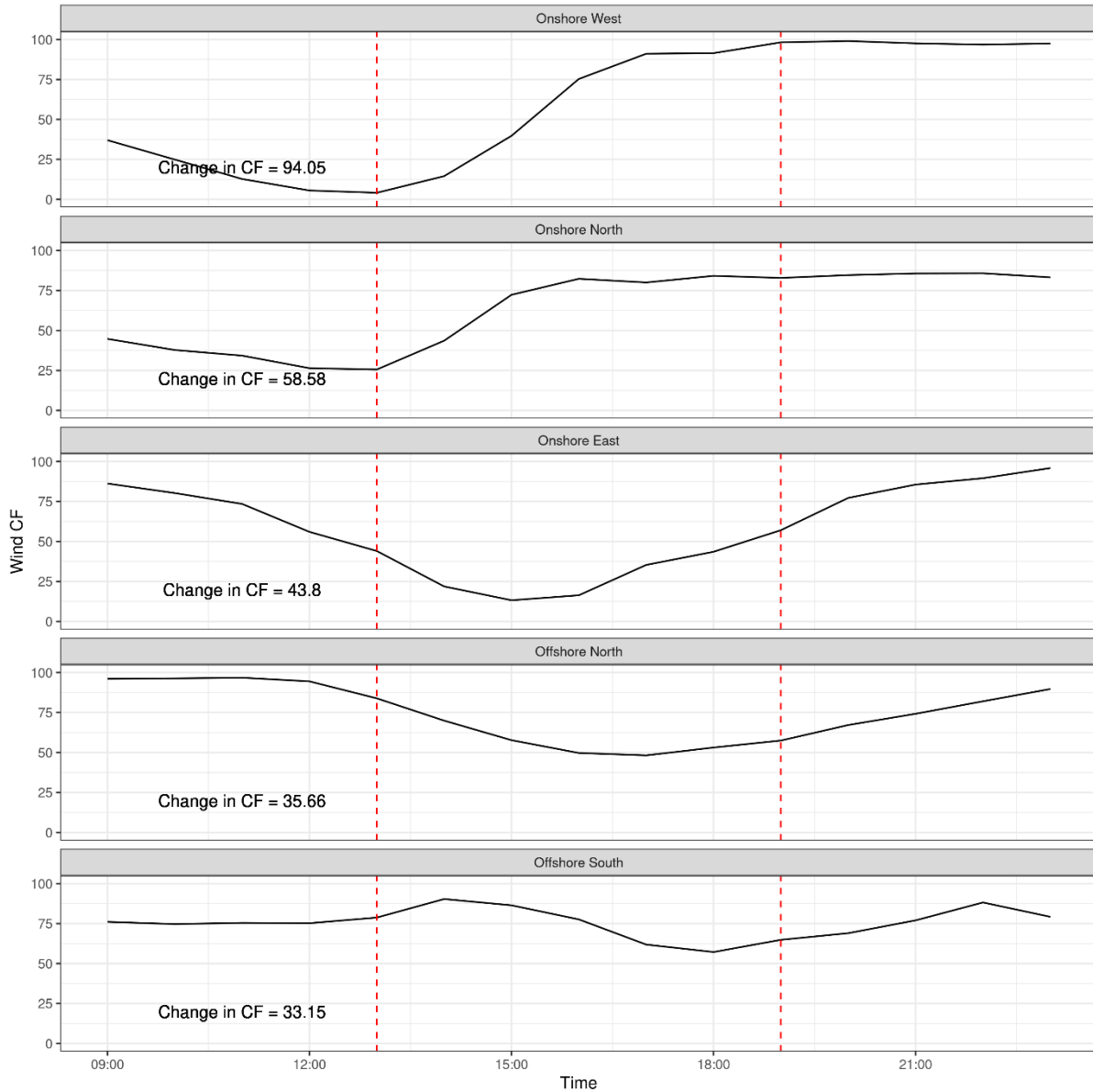
Appendix 11

The most extreme wind ramp event observed in a 6-hour time window in the 36-year timeseries for Onshore North (top row), occurred on the 3rd February 2011. The capacity factor change over the same time window for the four other regions are presented to provide context of conditions elsewhere in Great Britain.



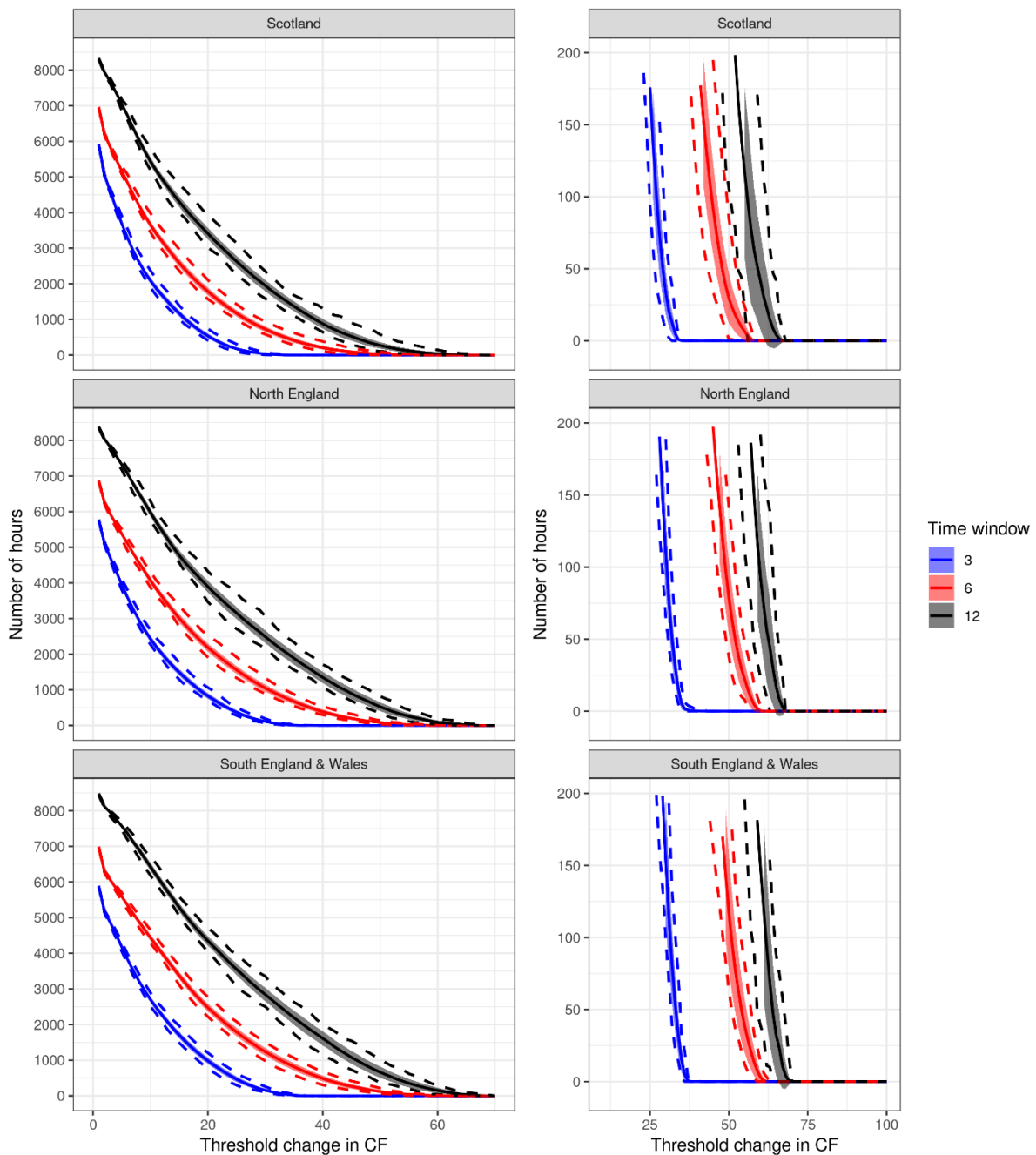
Appendix 12

The most extreme wind ramp event observed in a 6-hour time window in the 36-year timeseries for Onshore West (top row), occurred on the 24th December 1989. The capacity factor change over the same time window for the four other regions are presented to provide context of conditions elsewhere in Great Britain.



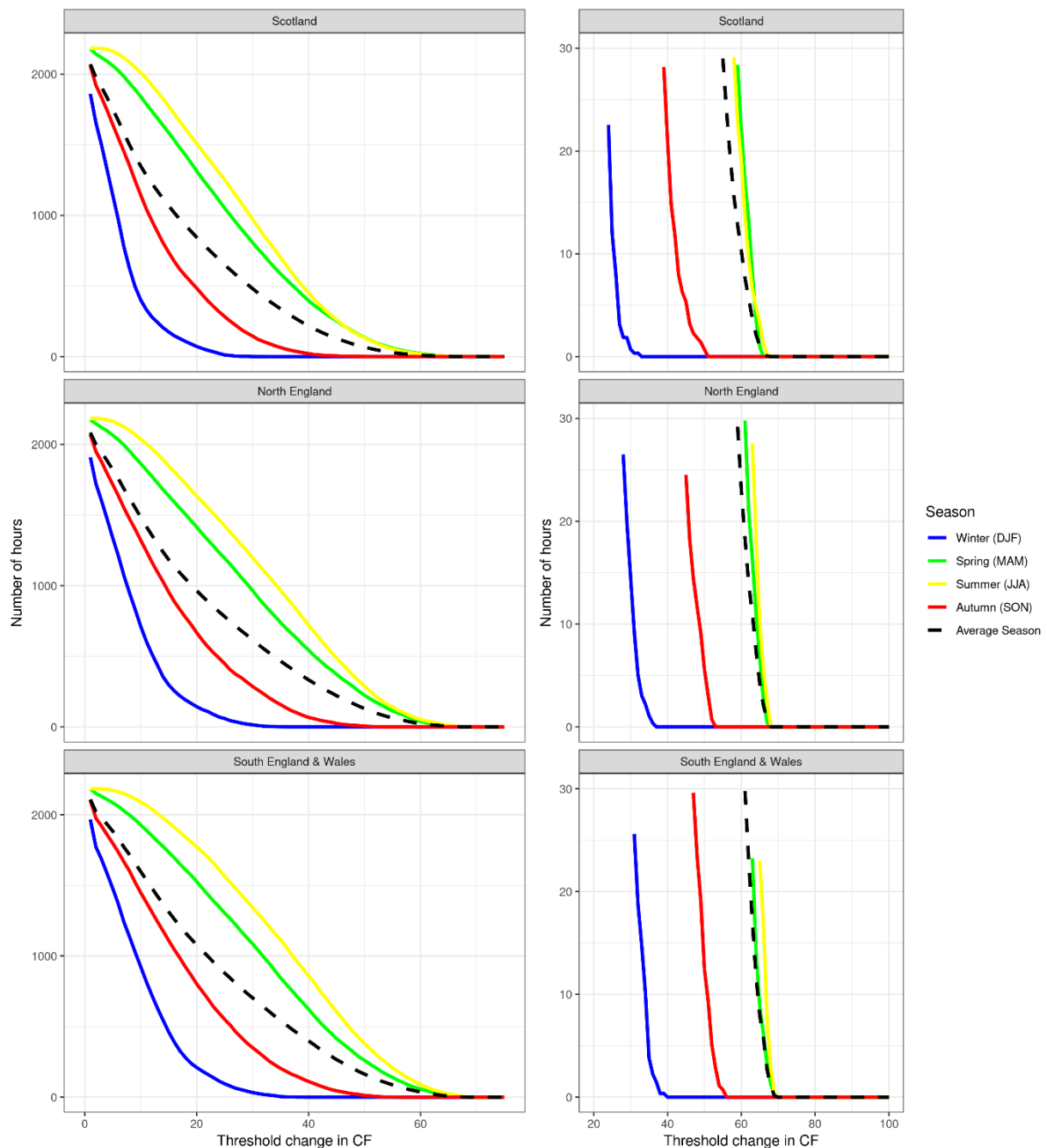
Appendix 13

The number of times (y-axis) that a solar ramp event reaches or exceeds a threshold of capacity factor change (x-axis) for three different time windows (3-, 6- and 12-hours), shown for each defined solar region. For each time window, the shaded area shows the frequency in a mean year ± 1 standard deviation and the dashed lines show the highest and lowest number that occurred in any one year. The right-hand panel presents an exploration of the less frequent ramping events for each time window or season i.e., focusing on events reaching a threshold change less than 200 times (number of hours) in an average year. In the right-hand panel plots, the shaded region deviates to the right of the mean line. This is the result of the plotting functionality in R when truncating a shaded region and therefore this plot should only be interpreted for y in (0,100) when observing the standard deviation around the mean.



Appendix 14

The number of times that a solar ramp event reaches or exceeds a threshold of capacity factor change (x-axis) for an average season and the four meteorological seasons (winter, spring, summer and autumn) in a 12-hour time window for each defined solar region. The right-hand panel presents an exploration of the less frequent ramping events for each time window or season i.e., focusing on events reaching a threshold change less than 30 times (number of hours) in an average year.



Appendix 15

Example solar ramping events observed in the Euro4 hindcast dataset in 'Scotland' for different time windows and return periods. The first column indicates the length of the time-window in which an event was observed. The second column indicates the return period i.e., number of years in between events. The third column indicates the observed return level (extremity of 'change in CF'). The fourth column indicates the date/time for the end of the window in which the event occurred.

	Time window (hours)	Return period (years)	Return level (change in CF)	Date-Time at end of window
1	1	1	11.67	27/05/1992 07:01
2	1	2	11.94	01/05/1984 08:01
3	1	5	12.33	06/08/1992 09:01
4	1	10	12.61	01/05/1995 09:01
5	1	20	13.06	18/05/2007 11:01
6	1	30	13.9	10/06/1983 15:01
7	3	1	32.89	21/06/1986 09:01
8	3	2	33.26	01/05/2011 09:01
9	3	5	33.62	30/04/2007 09:01
10	3	10	33.72	03/06/1997 09:01
11	3	20	34.2	26/04/1991 09:01
12	3	30	34.73	01/06/1997 09:01
13	6	1	56.17	27/06/1995 10:01
14	6	2	56.46	15/05/1980 20:01
15	6	5	56.79	12/06/1992 10:01
16	6	10	57.05	27/05/1992 10:01
17	6	20	57.38	17/05/1980 20:01
18	6	30	57.63	17/05/1980 10:01
19	12	1	63.09	03/06/1985 12:01
20	12	2	64.31	02/06/1985 12:01
21	12	5	64.85	01/06/1997 12:01
22	12	10	65.44	11/06/1992 12:01
23	12	20	65.84	22/06/1995 12:01
24	12	30	66.23	21/06/1986 12:01
25	24	1	61.54	14/05/2005 12:01
26	24	2	63.34	16/05/1988 12:01
27	24	5	64.6	06/06/1983 12:01
28	24	10	65.23	03/06/1997 12:01
29	24	20	65.84	22/06/1995 12:01
30	24	30	66.23	21/06/1986 12:01

Appendix 16

Example solar ramping events observed in the Euro4 hindcast dataset in 'North England' for different time windows and return periods. The first column indicates the length of the time-window in which an event was observed. The second column indicates the return period i.e., number of years in between events. The third column indicates the observed return level (extremity of 'change in CF'). The fourth column indicates the date/time for the end of the window in which the event occurred.

	Time window (hours)	Return period (years)	Return level (change in CF)	Date-Time at end of window
1	1	1	14.15	20/06/1998 09:01
2	1	2	15.05	07/05/1981 15:01
3	1	5	15.82	03/07/1996 13:01
4	1	10	16.15	05/07/2014 09:01
5	1	20	16.87	04/06/1999 11:01
6	1	30	17.38	05/08/2003 13:01
7	3	1	35.45	26/05/1986 18:01
8	3	2	36.63	24/05/1995 16:01
9	3	5	38.17	26/05/1986 10:01
10	3	10	39.28	31/07/1994 17:01
11	3	20	41.28	29/04/1987 16:01
12	3	30	41.85	05/07/2014 10:01
13	6	1	58.46	11/05/1980 19:01
14	6	2	58.84	06/06/1983 20:01
15	6	5	59.48	02/06/1985 10:01
16	6	10	59.73	13/05/1984 10:01
17	6	20	59.91	08/06/1996 10:01
18	6	30	60.14	28/05/1985 11:01
19	12	1	65.42	30/05/2009 12:01
20	12	2	66.17	27/06/1995 12:01
21	12	5	66.66	02/06/1985 12:01
22	12	10	66.83	13/06/1988 12:01
23	12	20	66.93	06/06/1983 12:01
24	12	30	66.93	06/06/1983 12:01
25	24	1	64.11	04/07/1983 12:01
26	24	2	65.26	26/05/1992 12:01
27	24	5	66.31	01/06/1979 12:01
28	24	10	66.66	02/06/1985 12:01
29	24	20	66.83	13/06/1988 12:01
30	24	30	66.93	06/06/1983 12:01

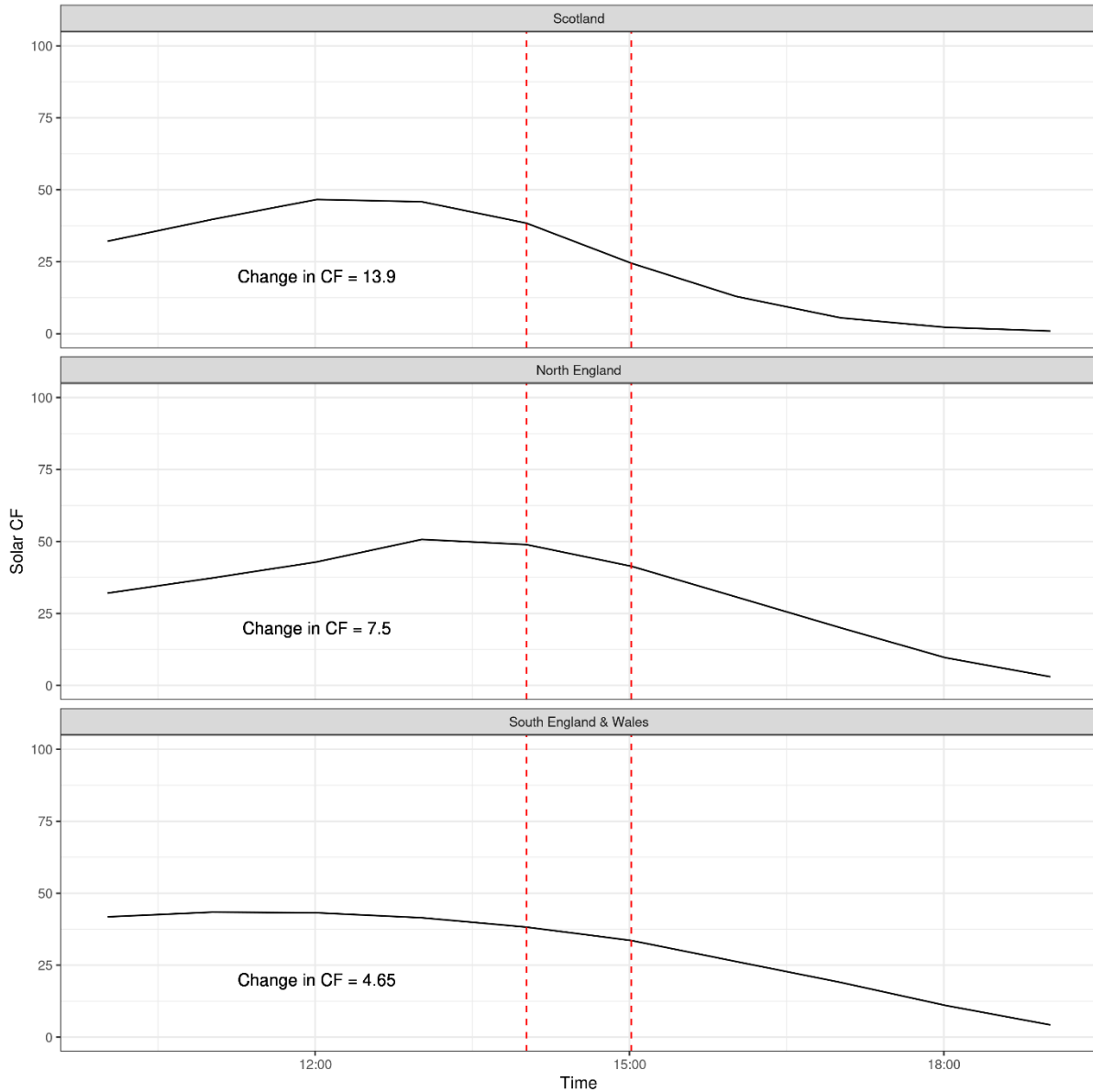
Appendix 17

Example solar ramping events observed in the Euro4 hindcast dataset in 'South England and Wales' for different time windows and return periods. The first column indicates the length of the time-window in which an event was observed. The second column indicates the return period i.e., number of years in between events. The third column indicates the observed return level (extremity of 'change in CF'). The fourth column indicates the date/time for the end of the window in which the event occurred.

	Time window (hours)	Return period (years)	Return level (change in CF)	Date-Time at end of window
1	1	1	12.75	11/06/1988 09:01
2	1	2	13	10/06/2000 17:01
3	1	5	13.31	26/04/1994 08:01
4	1	10	13.41	26/04/1994 16:01
5	1	20	13.51	01/05/1986 08:01
6	1	30	14.48	21/08/1980 09:01
7	3	1	35.88	24/04/1984 18:01
8	3	2	36.12	17/05/1992 09:01
9	3	5	36.64	19/07/1997 09:01
10	3	10	36.76	01/06/1985 08:01
11	3	20	37.04	26/04/1994 17:01
12	3	30	39.21	21/08/1980 10:01
13	6	1	59.89	04/06/2013 10:01
14	6	2	60.28	02/06/2009 10:01
15	6	5	60.55	12/06/1992 10:01
16	6	10	60.86	31/05/1985 10:01
17	6	20	61.53	30/05/1985 10:01
18	6	30	61.88	01/06/1985 10:01
19	12	1	66.89	15/07/2006 12:01
20	12	2	67.27	29/05/1997 12:01
21	12	5	67.67	12/06/1992 12:01
22	12	10	67.94	02/06/1985 12:01
23	12	20	68.42	01/06/1985 12:01
24	12	30	68.42	01/06/1985 12:01
25	24	1	65.57	04/07/1989 12:01
26	24	2	66.55	17/07/1996 12:01
27	24	5	67.24	16/06/1996 12:01
28	24	10	67.44	01/06/1997 12:01
29	24	20	67.67	12/06/1992 12:01
30	24	30	68.42	01/06/1985 12:01

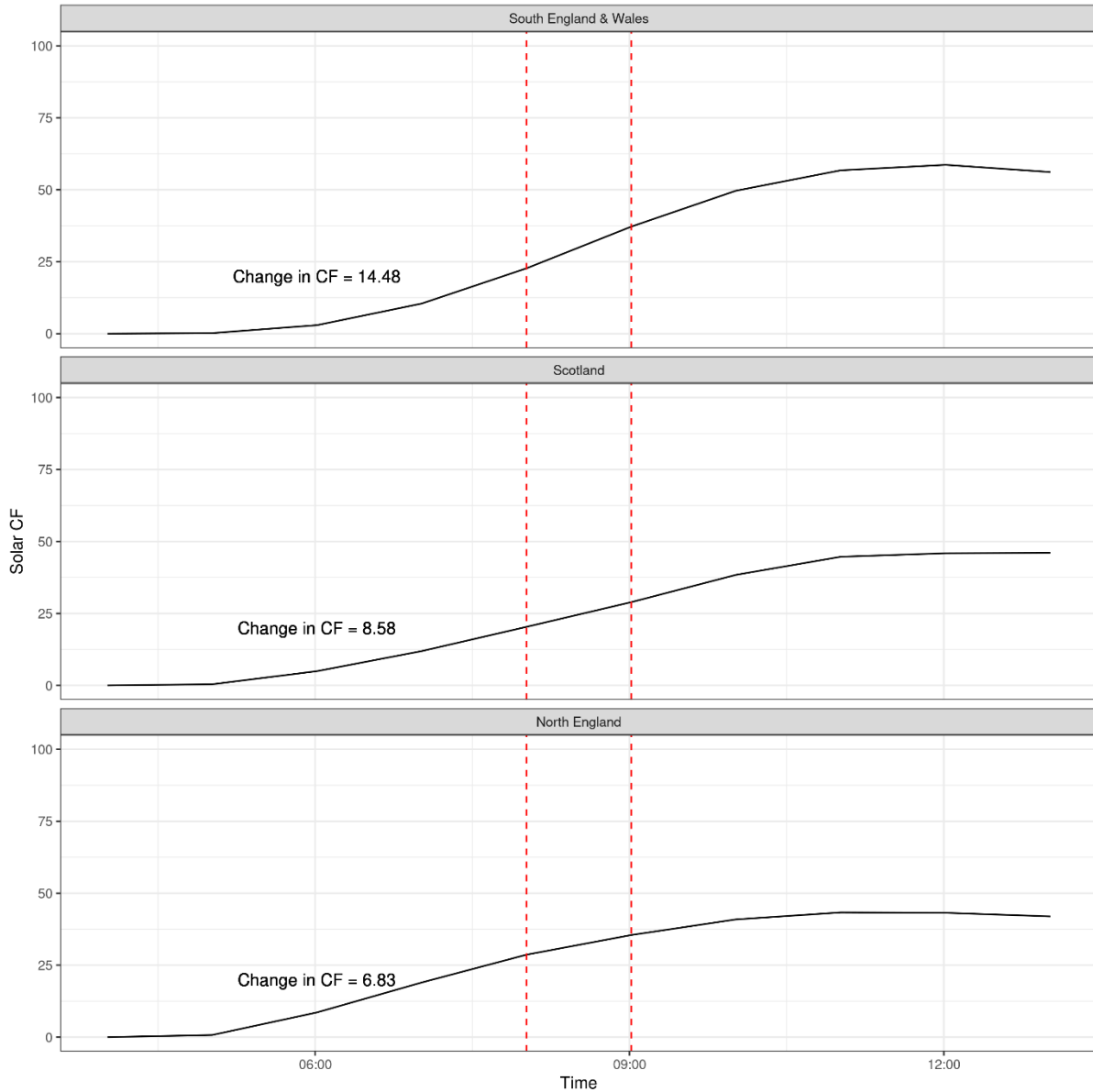
Appendix 18

The most extreme solar ramp event observed in a 1-hour time window in the 36-year timeseries for Scotland (top row), occurred on the 10th June 1983. The capacity factor change over the same time window for the four other regions are presented to provide context of conditions elsewhere in Great Britain.



Appendix 19

The most extreme solar ramp event observed in a 1-hour time window in the 36-year timeseries for South England and Wales (top row), occurred on the 21st August 1980. The capacity factor change over the same time window for the four other regions are presented to provide context of conditions elsewhere in Great Britain.



9 Addendum

Following discussions with the project Advisory Group, the following additional test of the data and methods were recommended:

1. An exploration of the sensitivity of the identified wind ramping events to the definition of the spatial region used;
2. A validation of the Euro4 wind capacity factor estimates and subsequent ramping event frequencies using observed 'true' wind generation data for the same period.

This addendum carries out these two additional tests. This will help to better understand the sensitivity and validity of the results of this report, as well as of the final ramping event dataset that will be produced in the next phase of the project. These additional tests focus on wind ramping events because these will be the focus of the next phase of the project (as discussed in Section 5).

Region sensitivity study

- 9.1 To explore the sensitivity of the identified wind ramping events to the definition of the spatial regions used, the 'Offshore South' region is divided into two to form 'Offshore South-East' and 'Offshore South-West' regions, as shown in Figure A1. This division of the region could have been done in any number of ways. For this exploration, an east-west divide is used similar to the east-west divide used onshore (see Figure 1a).

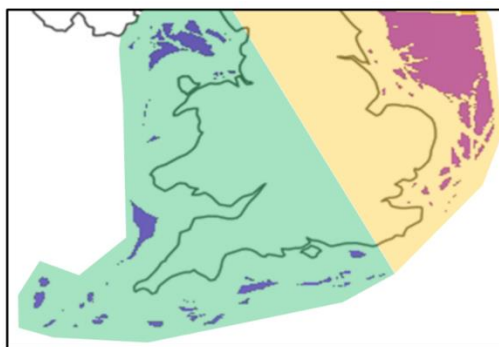


Figure A1: Map showing how the 'Offshore South' region has been divided into two to form 'Offshore South-East' (red region within yellow area) and 'Offshore South-West' (purple region within green area) regions for this sensitivity study.

In Section 4 it was shown how the Offshore South region experienced less extreme ramping events compared to other regions. It was hypothesised that this was because of the greater

spatial distribution of turbines over a wider area in this region. Dividing this region into two smaller regions, is therefore expected to have an overall impact on the frequency of extreme ramping events captured within the region. The aim of this sensitivity study is therefore to explore the magnitude of this effect, and ultimately whether this has an impact on the representation of extreme ramping events selected for the final dataset (in the next phase of the project). That is, are the extreme ramping events captured using the larger region representative of a combination of extreme events in both of the smaller regions? If so, the sensitivity to region choice is minimal. If not, this is a caveat for consideration when using the final dataset.

Figure A2 shows a comparison of the hourly regional average wind CF in each of the three regions (full Offshore South, Offshore South-East and Offshore South-West) for July 1979 (period chosen at random). This plot shows how fluctuations in wind CF in the three regions generally follows a similar pattern, albeit with slightly different magnitudes. It is also evident that the Offshore South-East region is more similar to the full Offshore South region, with the Offshore South-West region varying quite differently from the other two regions at times. This suggests that the South-East part of the region dominates the full Offshore South region, as may be expected by the overall larger area covered by this region (as shown in Figure A1).

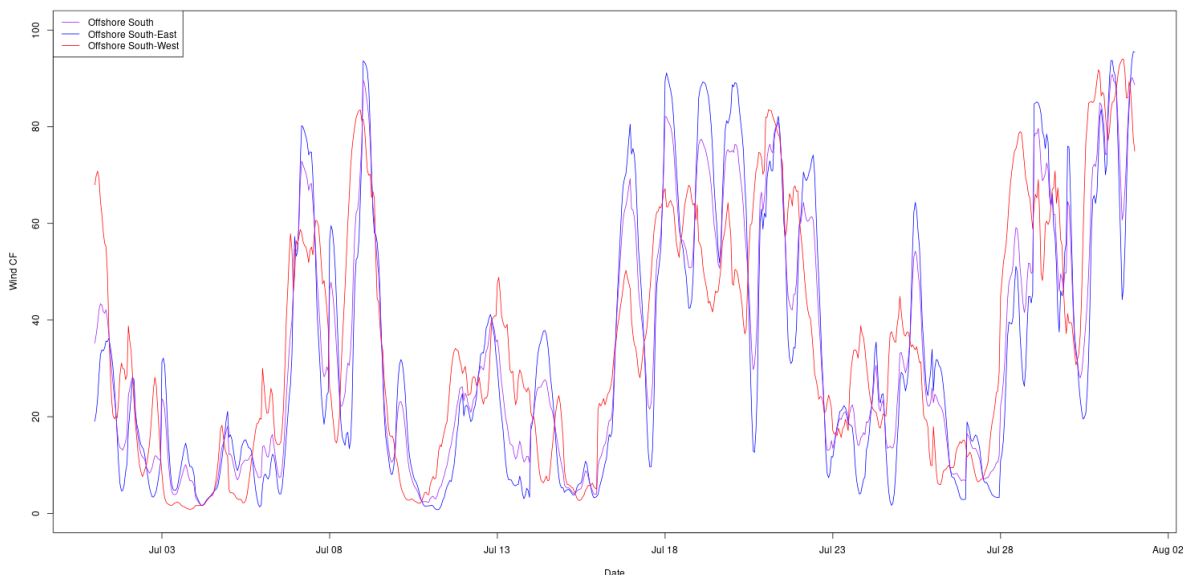


Figure A2: Time series plot comparing the hourly Wind CF calculated for the three regions ('Offshore South', 'Offshore South-East' and 'Offshore South-West') in July 1979.

Similar to the plots shown in earlier figures within this report, Figure A3 compares the frequency of ramping events of different sizes within the three regions. This shows how, as

was previously found, the smaller the region the more frequent the occurrence of larger ramping events (this is because there is less spatial diversification, and hence averaging, of the wind variability). This is captured in the relative high frequency of more extreme ramps in the Offshore South-East region (the least spatially diverse of the three regions), across all ΔCF thresholds. In addition, the Offshore South-West region has slightly higher frequency of very extreme ramping events in larger time windows when compared to the more spatially diverse Offshore South region.

This shows that the definition of the regions does indeed have an impact on the quantified *absolute* magnitude of ramping events. However, as the aim of this project is to develop a dataset of adverse weather scenarios for electricity systems by selecting relevant events at different *relative* extreme levels (rather than absolute) this sensitivity is only relevant if it has an impact on the definition of a relative 'relevant event'.

To explore this, Figure A4 shows two examples of time slices during which extreme ramping events occur within the full Offshore South region. These plots also compare how the wind CF varies over the same period within the other two smaller regions. This shows how, for example, during the most extreme (rank=1) 3-hour wind ramping event in the full Offshore South region, a similarly relatively extreme (rank=11) event is occurring in the Offshore South-East region, but a relatively more weak (rank=943) event is occurring in the Offshore South-West region. Conversely, during the most extreme (rank=1) 24-hour wind ramping event in the full Offshore South region, a similarly relatively extreme (rank=7) event is occurring in the Offshore South-West region, but a more relatively weak (rank=178) event is occurring in the Offshore South-East region.

Figure A4 therefore indicates that selecting relevant extreme ramping events for the dataset in the next phase of the project using the 'Offshore South' region definition, will provide ramping events that are relevant for this region as a whole but not necessarily relevant for all smaller areas within this region. This is an important caveat of the dataset that must be communicated. However, Figure A4 also indicates that changing the definition of the regions and using the smaller regions to select relevant relatively extreme events for the dataset (e.g. the top 10) would indeed provide extreme events seen in the larger region (i.e. the events shown in the plots). Similar results are found in other time windows (not shown). This gives confidence that the events selected based on any given region definition will include relevant extreme adverse weather scenarios for all regions of the UK.

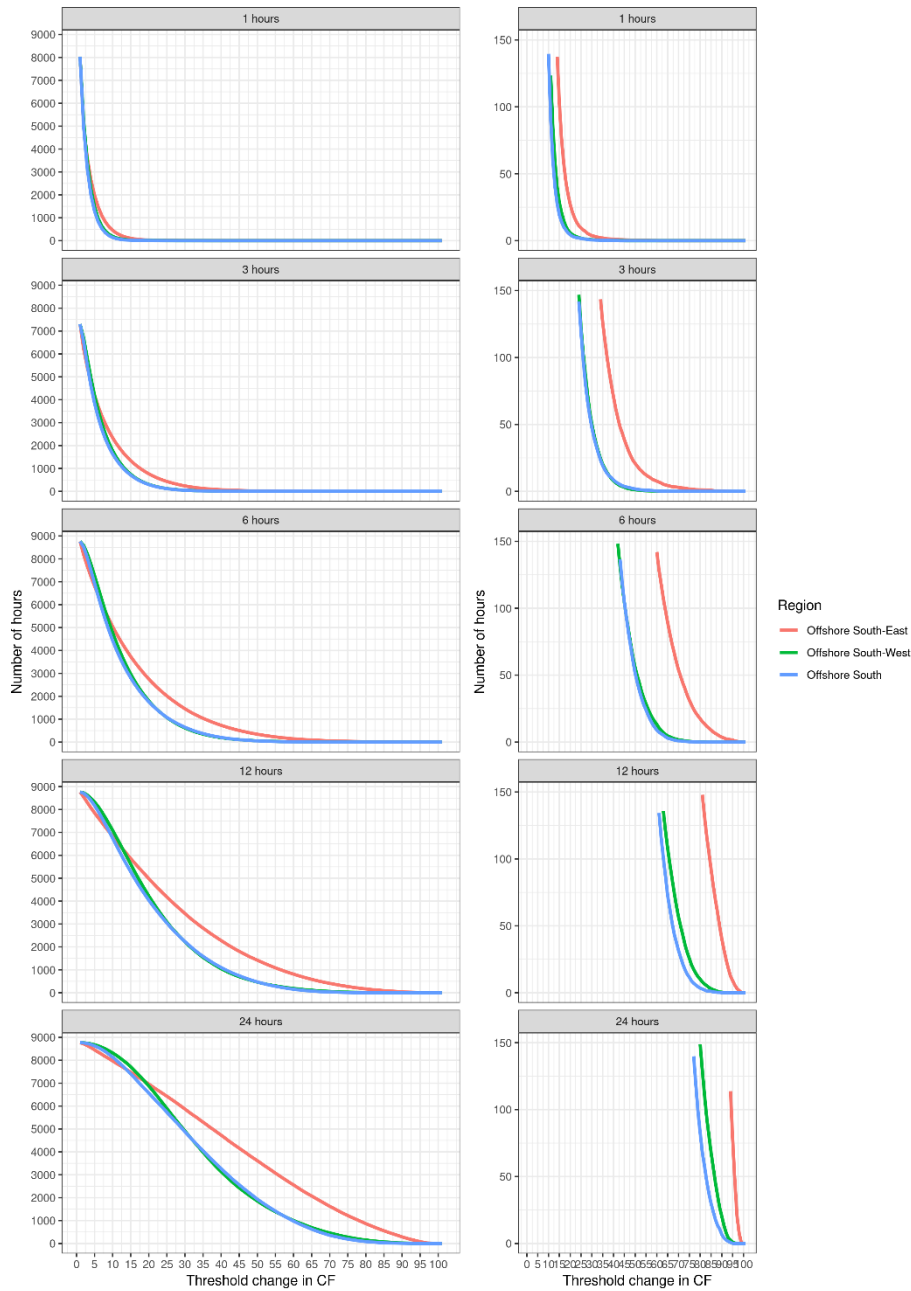
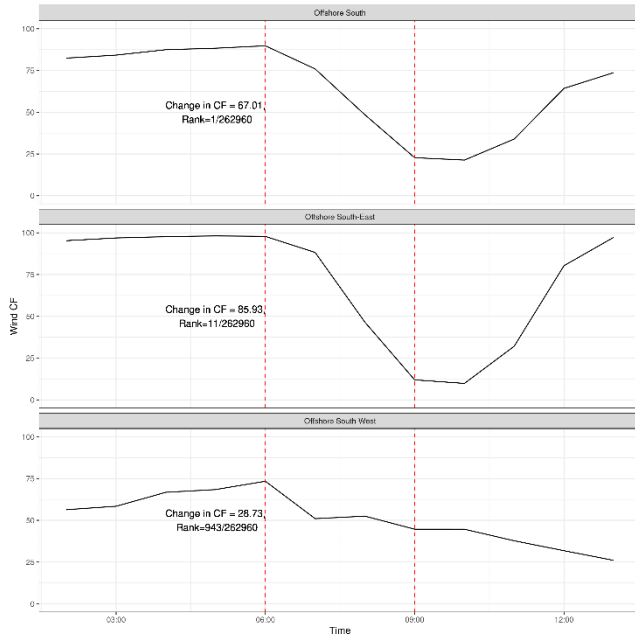


Figure A3: The number of hours in an average year (y-axis) that a ramp event is observed reaching or exceeding a threshold of ΔCF (x-axis). Each line on the plot represents a different defined region with a row per a time window – identified in the top grey bar. The right-hand panel presents an exploration of the less frequent ramping events for each time window i.e., focusing on events reaching a threshold change less than 150 times (number of hours) in an average year.

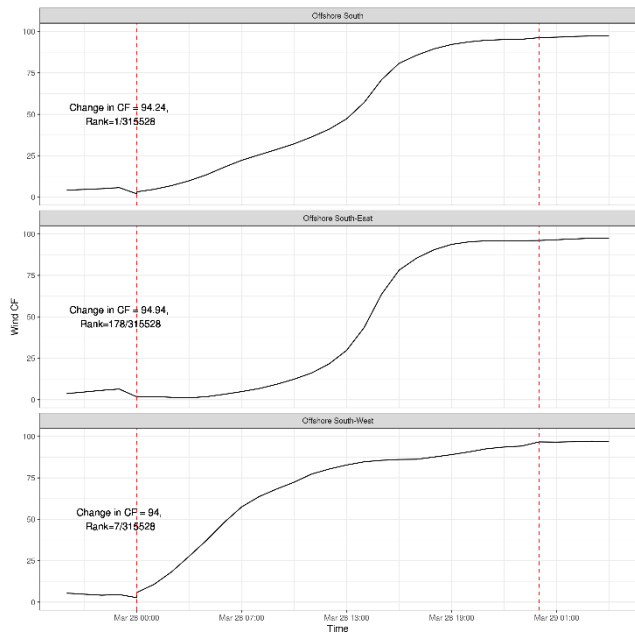
It must also be noted that the final dataset of adverse ramping events will provide high-resolution (4km, hourly) wind speed data across the UK and North Sea. This will allow for the user of the data to explore events within any desired region, as small as up to a 4km grid cell. Based on the results of this sensitivity study, it is advised that the user does, however, explore

whether the level of extremity of the event given in the dataset for the defined regions (e.g. a 1 in 100 year event in the Offshore South region) is consistent in their smaller region of interest.



In the next phase of the project, the five wind regions used in this report (see Figure 1) will continue to be used. However, to help facilitate user exploration of smaller sub-regions, we will share a high number of ramping events at each extreme level (approximately 10) to ensure many different variations in conditions across each region are captured within the final dataset.

Figure A4: Time series plots comparing the wind CF in each of the three regions ('Offshore South', 'Offshore South-East' and 'Offshore South-West') during the most extreme 3-hour (left) and 24-hour (right) ramping events experienced in the full Offshore South region within the study period. In each case, the window over which the ramping event occurs is shown by the dashed red lines. The maximum change in CF over the window is given, as well as the rank (extremity) of the event.



Euro4 wind ramping validation

The results presented in this report are derived using bias corrected Euro4 100m wind data, as well as a simplified energy system model, based on mathematical representations of wind power curves (see Section 3.1 for full description). It is therefore important to validate the data and the simplified energy system models used against observed generation data. This helps to understand how well this data and the modelling techniques used are able to provide realistic representations of the real world.

Similar to Cannon et al. (2015), this is achieved by directly comparing the wind generation and the subsequent frequency of wind ramping events of different magnitudes derived from the modelled analysis, with those in the observed record.

For this, the observed record is represented using the ENTSO-E transparency platform¹¹ wind generation data. This product is commonly used as a validation tool in the energy literature, and is available from January 2015. The Euro4 hindcast runs to the end of June 2015, hence this 6 month overlap with the ENTO-E observed record is used for validation (1st January – 30th June 2015). Other observed energy data records were explored, but none were found to extended further back to pre-2015.

To allow for a direct comparison, the simplified energy system model used in this analysis is modified to represent the actual location and quantity of installed wind turbine capacity, rather than the potential location of future turbines (as was used in the main analysis in this report). This information is derived from the ‘thewindpower.net’ turbine information as of 2017 (the closest year to 2015 available for our use). For both datasets (modelled and observed), hourly wind generation is converted to hourly wind capacity factor by dividing through by the maximum wind generation in the 6 month period in that dataset. This approach is taken (rather than dividing by the installed capacity) due to the uncertain and inconsistent estimates of GB installed capacity available. This process provides hourly modelled and observed wind CF data for 1st January - 30th June 2015 for validation. In addition, this is calculated separately for the onshore and offshore regions, to allow for them to be validated separately.

Figure A5 directly compares the temporal variability of observed and modelled hourly wind capacity factors for this 6 month period. These plots show how the observed data is generally well captured by the model in the offshore region, although the modelled data marginally over estimates the most extreme CFs (panel a). In comparison, the modelled onshore CFs,

¹¹ <https://www.entsoe.eu/data/transparency-platform/> (Accessed 29/11/2021)

estimated using the Bloomfield et al. (2019) turbine power curves (representative of type 1, 2 and 3 turbines from the International Electrotechnical Commission (IEC) wind speed classification respectively (IEC, 2005)) are consistently larger than those in the observed record, throughout the 6 month period (panel b).

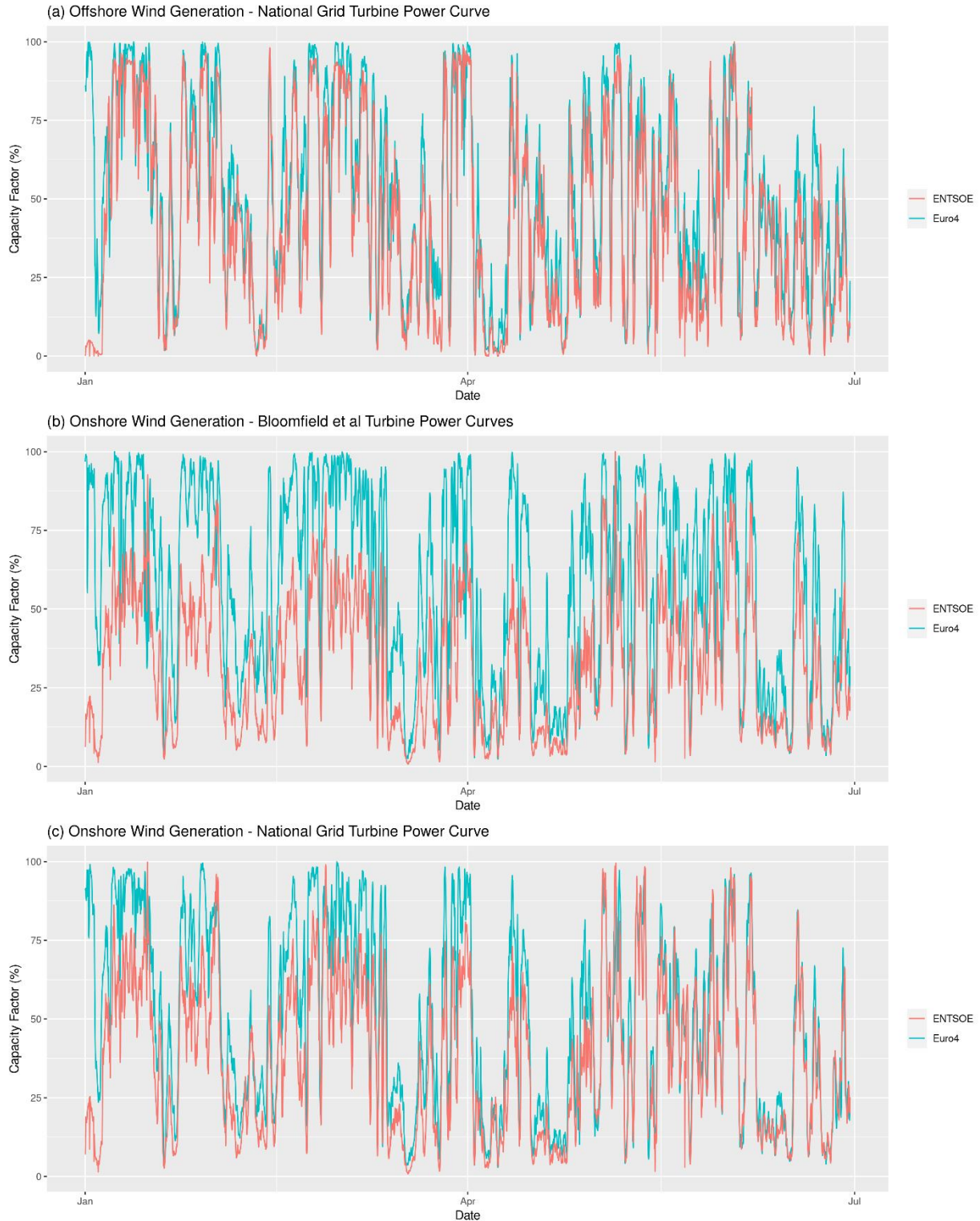


Figure A5: Time series plots comparing modelled (Euro4) and observed (ENTSOE) wind capacity factor for the validation period (01/01/2015-30/06/2015), for (a) the offshore region, (b) the onshore region using the IEC/Bloomfield et al. (2019) turbine power curves, and (c) the onshore regions using the National Grid onshore turbine power curve (see Figure A6 for a comparison of these turbine curves).

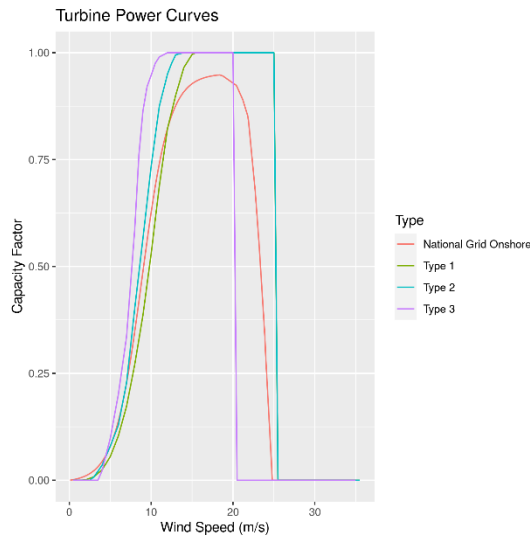


Figure A6: A comparison of the different wind turbine power curves used in this analysis: the National Grid onshore curve, and the International Electrotechnical Commission type 1, 2 and 3 turbines (used by Bloomfield et al., 2019). These different turbine power curves represent different relationships between 100m wind speed (x-axis) and wind capacity factor (y-axis).

The inconsistency in Figure A5 (b) is thought to be due to the wind turbine power curve used in the modelling. Figure A6 shows a comparison of the turbine curves used in the analysis in the main body of this report (the IEC type 1, 2 and 3 turbines, as used by Bloomfield et al., 2019), and an alternative curve provide by National Grid, better suited to representing a wind farm rather than a single wind turbine. Throughout GB the IEC turbine type 3 is used, and hence these is a considerable difference in the two potential turbine curves (IEC type 3 – purple, and National Grid – red).

Figure A5 (c) shows an equivalent comparison to (b), but now using the National Grid onshore power curve. This greatly improves the consistency between the observed and modelled data, particularly in the second half of the 6 month period. The modelled data has a consistent level of installed wind capacity throughout the period (representative of 2017), whereas the observed record will capture how the installed capacity actually changed throughout the 2015 validation period (i.e. due to wind farms going on and offline). It is therefore likely that this change in the consistency between the datasets is due to the installation of additional wind capacity in approximately April 2015, bringing the installed level closer to the 2017 system

used in the model. For example, this could in part be due to the 15MW Jack's Lane Wind Farm, which came online in April 2015¹².

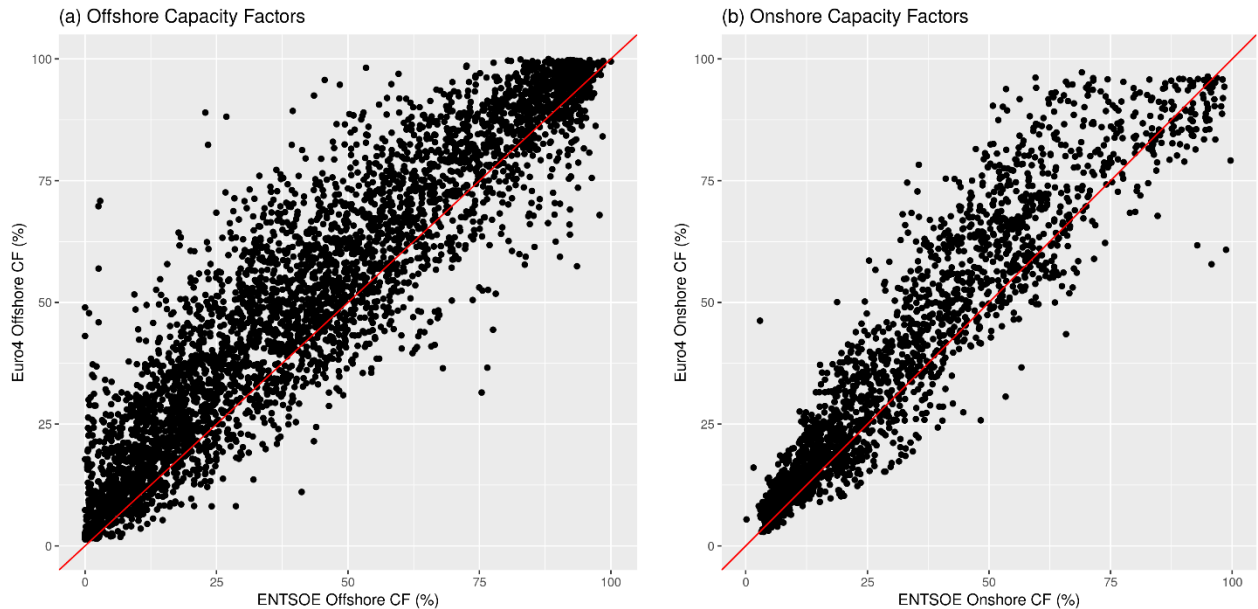


Figure A7: Scatter plots comparing the observed (x-axis) and modelled (y-axis) hourly wind capacity factors for (a) the offshore region over the period 01/01/2015-30/06/2015, and (b) the onshore region over the period 01/04/2015-30/06/2015 using the National Grid onshore turbine power curve. The red line shows the line of $y=x$ (i.e. perfect agreement).

Figure A7 shows a comparison of observed and modelled hourly wind CF in the offshore and onshore regions, in the form of scatter plots (where each point is an hour within the validation period). This is presented for the full 6 months for the offshore region, and for the more consistent 3 months for the onshore region (using the National Grid turbine power curve). Similar to Figure A5, these plots show generally good consistency between the observed and modelled hourly CF values. In both regions, the model tends to give slightly higher CF values. There is also a scatter of points around the $y=x$ line, meaning that the model sometimes over/underestimates the observed CF.

This could be partly due to the observed record including human-driven factors such as curtailment and maintenance, while the model only captures weather driven variations in CF. In addition, the modelled analysis is based on a miss-match of information (e.g. weather from 2015 and installed capacity of 2017), and methodological approximations (e.g. dividing by the maximum wind generation rather than the installed capacity, which will change over time in

¹² <http://www.jackslanewindfarm.co.uk/about-the-project/jacks-lane-wind-farm/> (Accessed 29/11/2021)

the observed record). Further it should be noted that this validation is based on only a short 6-month overlapping time period.

Overall, however, Figure A7 gives good confidence that the underlying Euro4 100m wind speed data, and simplified energy system model validate well, and are generally able to capture the observed wind CF record. This good validation is achieved by using the National Grid turbine power curve onshore, hence it is recommended that this power curve be used in future phases of this project (i.e. when developing the dataset of short-duration ramping events). Note that the results in the main body of this report are based on the alternative power curve.

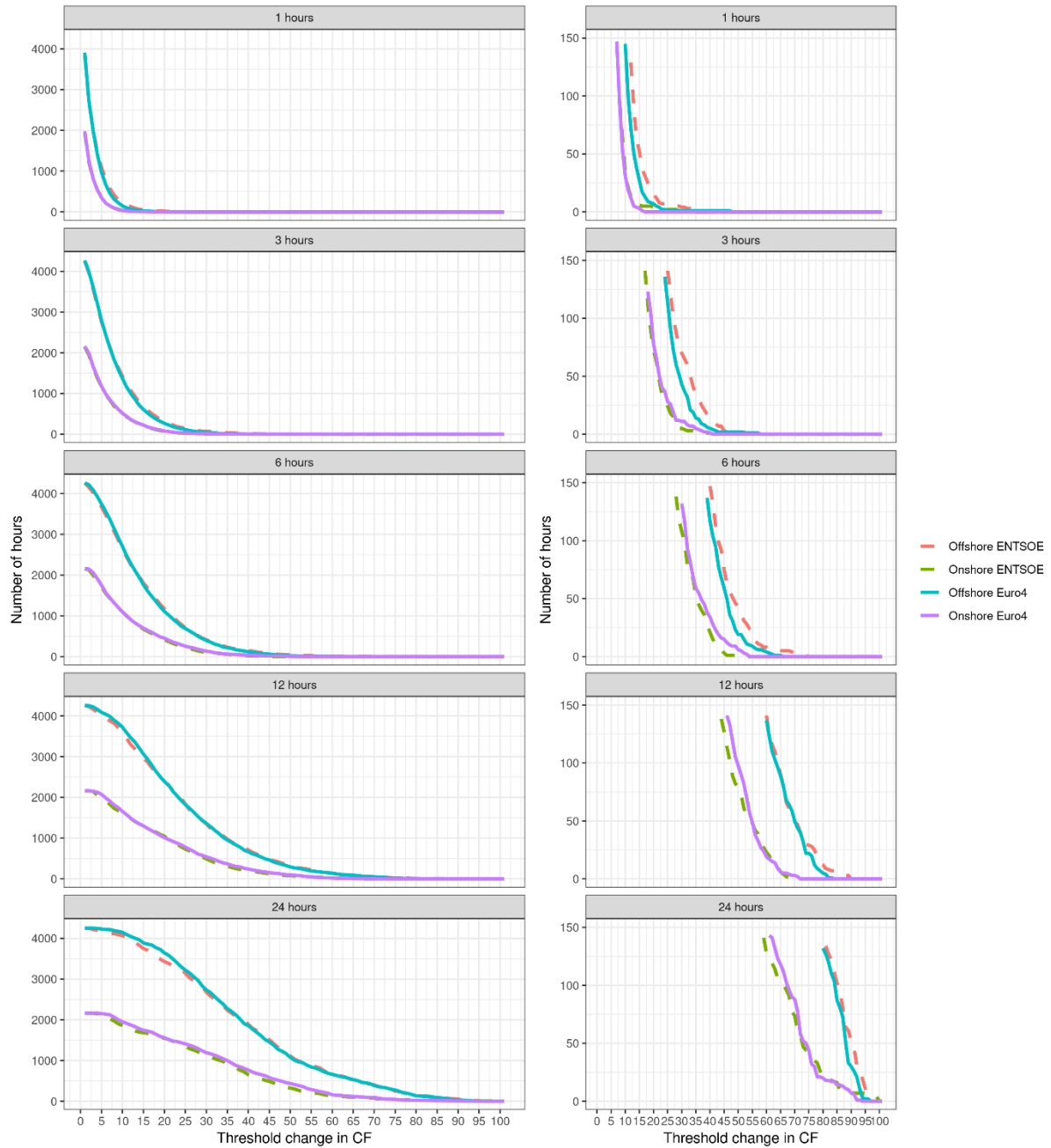


Figure A8: The number of hours in the validation period (y-axis) that a ramp event is observed reaching or exceeding a threshold of ΔCF (x-axis). The solid blue and dashed red lines represent the 6-month offshore validation period in the modelled and observed record respectively. The solid purple and green dashed lines represent the 3-month onshore validation period in the modelled and observed record respectively. Each row represents a different time window – identified in the top grey bar. The right-hand panel presents an exploration of the less frequent ramping events for each time window i.e., focusing on events reaching a threshold change less than 150 times (number of hours) in the validation period.

Figure A8 presents a validation of the subsequent ability of the model to represent the observed frequency of ramping events of different magnitudes. This figure indicates that, both in the offshore and onshore regions (when the National grid turbine power curve is used), the observed frequency of ramping events of all magnitudes are well captured by the

model. This is even generally the case for the most extreme ramping events (as shown in the right panel of Figure A8).

In conclusion, it has been shown that, when using the most appropriate wind turbine power curve, the modelled wind CFs and ramping events (and hence Euro4 wind data) validate well against the observed record. This indicates the need to adapt the approach in future phases to using the National Grid turbine onshore.